Title
Cancer-Specific Retargeting of BAF Complexes by a Prion-like Domain

Journal
Cell, 171(1)

ISSN
0092-8674

Authors
Boulay, Gaylor
Sandoval, Gabriel J
Riggi, Nicolo
et al.

Publication Date
2017-09-01

DOI
10.1016/j.cell.2017.07.036

Peer reviewed

HHS Public Access

Author manuscript

Cell. Author manuscript; available in PMC 2019 October 14.

Published in final edited form as:

Cell. 2017 September 21; 171(1): 163–178.e19. doi:10.1016/j.cell.2017.07.036.

Cancer-Specific Retargeting of BAF Complexes by a Prion-like Domain

Gaylor Boulay[1,3,5,6], **Gabriel J. Sandoval**[2,3,6], **Nicolo Riggi**[4], **Sowmya Iyer**[1], **Rémi Buisson**[5], **Beverly Naigles**[1,5], **Mary, E. Awad**[1,5], **Shruthi Rengarajan**[1,5], **Angela Volorio**[1,4,5], **Matthew J. McBride**[2,3], **Liliane C. Broye**[4], **Lee Zou**[5], **Ivan Stamenkovic**[4], **Cigall Kadoch**[2,3,7,*], **Miguel N. Rivera**[1,3,5,7,8,*]

[1]Department of Pathology, Massachusetts General Hospital and Harvard Medical School, Boston, MA 02114, USA [2]Dana-Farber Cancer Institute and Harvard Medical School, Boston, MA 02215, USA [3]Broad Institute of Harvard and MIT, Cambridge, MA 02142, USA [4]Institute of Pathology, Centre Hospitalier Universitaire Vaudois, Faculty of Biology and Medicine, University of Lausanne, 1011 Lausanne, Switzerland [5]Center for Cancer Research, Massachusetts General Hospital and Harvard Medical School, Charlestown, MA 02129, USA [6]These authors contributed equally [7]Senior author [8]Lead Contact

SUMMARY

Alterations in transcriptional regulators can orchestrate oncogenic gene expression programs in cancer. Here, we show that the BRG1/BRM-associated factor (BAF) chromatin remodeling complex, which is mutated in over 20% of human tumors, interacts with EWSR1, a member of a family of proteins with prion-like domains (PrLD) that are frequent partners in oncogenic fusions with transcription factors. In Ewing sarcoma, we find that the BAF complex is recruited by the EWS-FLI1 fusion protein to tumor-specific enhancers and contributes to target gene activation. This process is a neomorphic property of EWS-FLI1 compared to wild-type FLI1 and depends on tyrosine residues that are necessary for phase transitions of the EWSR1 prion-like domain. Furthermore, fusion of short fragments of EWSR1 to FLI1 is sufficient to recapitulate BAF complex retargeting and EWS-FLI1 activities. Our studies thus demonstrate that the physical properties of prion-like domains can retarget critical chromatin regulatory complexes to establish and maintain oncogenic gene expression programs.

In Brief

*Correspondence: cigall_kadoch@dfci.harvard.edu (C.K.), mnrivera@mgh.harvard.edu (M.N.R.) .

AUTHOR CONTRIBUTIONS

G.B., G.J.S., C.K., and M.N.R. designed the study and wrote the manuscript. G.B., G.J.S., N.R., R.B., B.N., M.E.A., S.R., A.V., and M.J.M. performed the experiments. S.I., G.B., and M.N.R. conducted bioinformatics analyses. N.R., L.C.B., L.Z., and I.S. provided necessary reagents and conceptual advice.

SUPPLEMENTAL INFORMATION

Supplemental Information includes seven figures and one table and can be found with this article online at http://dx.doi.org/10.1016Zj.celL2017.07.036.

Phase transition properties of a prion-like domain in an oncogenic fusion protein are critical for retargeting BAF chromatin remodeling complexes and activating enhancers, thereby driving the transcriptional program that promotes Ewing sarcoma.

Graphical Abstract

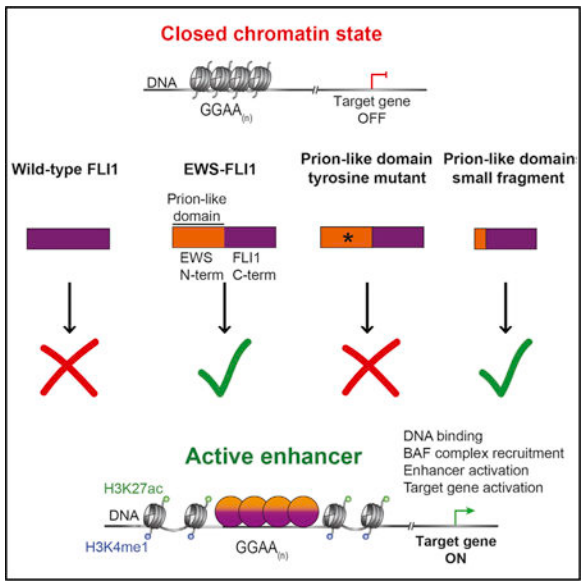

INTRODUCTION

Temporal and spatial regulation of gene expression plays a fundamental role in directing cell identity and proliferation in both normal tissues and in human disease. The striking number of genetic alterations in genes encoding transcription factors, chromatin modifiers, and histones that have been uncovered in recent whole-exome sequencing efforts have further highlighted the importance of gene regulation in cancer (Lander, 2011). Whereas these alterations can have profound consequences on cancer-specific gene expression, their precise mechanisms of action, in most cases, remain poorly understood.

In contrast to most adult tumor types, pediatric cancers are often driven by a limited number of genetic alterations (Lawrence et al., 2013). Pathognomonic chromosomal translocations represent an important class of these abnormalities and often lead to the formation of oncogenic fusion proteins that involve transcription factors or transcriptional regulators. One of the most well-characterized translocations results in the fusion of the EWSR1 gene and the FLI1 E-Twenty Six (ETS) transcription factor in Ewing sarcoma, the second most common pediatric bone cancer (Delattre et al., 1992). The EWS-FLI1 oncogenic fusion protein is often the only genetic alteration in these tumors (Brohl et al., 2014; Crompton et al., 2014; Tirode et al., 2014) and operates as an aberrant transcription factor containing the ETS DNA-binding domain of FLI1. EWSR1 has been linked to transcriptional activation and RNA binding (Kovar, 2011), yet its contribution to the function of EWS-FLI1 remains poorly defined.

Several studies have shown that EWS-FLI1 is necessary for Ewing sarcoma tumorigenicity (Herrero-Martin et al., 2011) and is sufficient for transformation of mesenchymal stem cells (MSCs) (Riggi et al., 2005, 2008). More recently, EWS-FLI1 has been shown to be a major determinant of genome-wide chromatin states in Ewing sarcoma (Riggi et al., 2014; Tomazou et al., 2015). Strikingly, EWS-FLI1 is able to activate a large set of target genes by operating as a pioneer factor at GGAA micro-satellite repeats and inducing active enhancers de novo starting from a closed chromatin conformation (Gangwal et al., 2008; Guillon et al., 2009; Patel et al., 2012; Riggi et al., 2014). This process of enhancer activation requires major restructuring of the chromatin environment, suggesting the participation of chromatin remodeling proteins that have yet to be defined.

The mammalian switch/sucrose non-fermentable (SWI/SNF) (or BAF, for BRG1/BRM-associated factor) complex is an ATP-dependent chromatin remodeler composed of 12–15 subunits that regulates genomic architecture and DNA accessibility (Ka-doch and Crabtree, 2015). Recent exome-sequencing studies have revealed that the genes encoding BAF complex subunits are recurrently mutated in over 20% of human cancers (Kadoch et al., 2013). Interestingly, specific subunits appear to be mutated in different cancer subtypes, suggesting tissue-specific functions (Kadoch and Crabtree, 2015; Kadoch et al., 2013; Roberts et al., 2002; Versteege et al., 1998). The high frequency of alterations in BAF complex subunits across a range of tumor types points to their critical role in controlling chromatin architecture and gene expression in cancer (Kadoch and Crabtree, 2015).

Using an unbiased mass spectrometry approach, we now show that BAF complexes interact with the wild-type protein EWSR1 in several cell types and with the EWS-FLI1 fusion protein in Ewing sarcoma. The BAF complex is specifically recruited by EWS-FLI1 to tumor-specific GGAA repeat microsatellites and is necessary for the activation of target genes. Remarkably, the ability to recruit BAF complexes and activate enhancers de novo at these repeat sites is a neomorphic property of EWS-FLI1 that depends on tyrosine residues in the EWSR1 prion-like domain, which are necessary for its interaction with wild-type EWSR1 and for its phase transition properties in vitro. These observations expand the set of human cancers in which BAF complex mistargeting contributes to oncogenesis beyond settings in which BAF complex genes themselves are mutated and show that recruitment via a prion-like domain is a powerful means of retargeting critical chromatin regulatory complexes to tumor-specific loci.

RESULTS

BAF Complexes Interact with Wild-Type EWSR1 and the Fusion Protein EWS-FLI1

BAF complexes are combinatorially assembled from a set of ubiquitously expressed core subunits as well as many cell-type- and context-specific subunits that give rise to an extensive diversity of complex configurations. In order to identify the constellation of BAF complex subunits and associated proteins, we performed endogenous capture of BAF complexes via anti-BRG1 immunoprecipitation followed by proteomic mass spectrometry in several cell types. Notably, these experiments revealed substantial enrichment of peptides corresponding to the EWSR1 protein, among several other previously unidentified proteins (Figure 1A). EWSR1 has been linked to several cellular processes, but most notably it has

been shown to be directly involved in gene regulation as a frequent partner in oncogenic fusion proteins with transcription factors, such as the EWS- FLI1 protein in Ewing sarcoma (Mertens et al., 2016). Given the strong connection between BAF and gene regulation in cancer, we proceeded to confirm whether EWSR1 as well as the EWS-FLI1 fusion protein can interact with BAF complexes. Immunoprecipitation experiments using antibodies specific for BRG1 performed on nuclear extracts isolated from EWSR1 wild-type cells (SAOS2 and U2OS) or EWS-FLI1-positive Ewing sarcoma cell lines revealed that both EWSR1 and the EWS-FLI1 fusion protein interact with BAF complexes (Figure 1B). Reciprocal immunoprecipitation experiments using an antibody specific for EWSR1 confirmed these interactions (Figure S1A). Similar experiments using antibodies specific to additional BAF complex subunits, BAF155 and SS18, also confirmed these interactions with EWS-FLI1 in Ewing sarcoma (Figure S1B).

To further characterize the interaction of EWS-FLI1 with BAF complexes, we performed immunodepletion experiments using an anti-BRG1 antibody in SK-N-MC Ewing sarcoma cell nuclear extracts to determine the relative fraction of EWS-FLI1 bound to BAF complexes. We found that EWS-FLI1 was significantly depleted from nuclear lysates over three rounds of anti-BRG1 immunoprecipitation, suggesting that a high percentage of total nuclear EWS-FLI1 associates with BAF complexes (Figure 1C). Reciprocal immunodepletion experiments using an EWSR1 antibody were only able to slightly deplete BAF complex components, indicating that only a small percentage of total BAF complexes are bound to EWS-FLI1 and wild-type EWSR1 (Figure S1C), consistent with genome-wide activities for this chromatin remodeling complex that are independent of these proteins. This was further substantiated by density sedimentation experiments, which showed that neither EWSR1 nor EWS-FLI1 were core members of the BAF complex (Figure S1D). Similarly, urea denaturation studies showed that EWSR1 interactions with BAF complex subunits were decreased at ~0.5 M urea (Figure S1E) and were thus weaker than those observed between core BAF complex members (≥2.5 M urea; Kadoch and Crabtree, 2013). Taken together, these data demonstrate that both wild-type EWSR1 and the oncogenic fusion protein EWS-FLI1 interact with BAF complexes in a transient manner.

EWS-FLI1 Recruits BAF Complexes to Tumor-Specific GGAA Microsatellite Repeat Enhancers to Activate Target Gene Expression

Owing to the biochemical interaction between BAF complexes and EWS-FLI1, we next sought to determine whether BAF complexes cooperate with EWS-FLI1 to regulate gene expression in Ewing sarcoma. We recently demonstrated that EWS-FLI1 operates as a pioneer factor to induce tumor-specific de novo enhancers at GGAA microsatellite repeats (Riggi et al., 2014), a process that may involve significant redistribution of chromatin remodeling complexes that directly govern DNA accessibility, such as BAF (Phelan et al., 1999). To address a potential collaborative role in this process, we performed chromatin immunoprecipitation followed by high-throughput DNA sequencing (ChIP-seq) studies to localize BAF complexes and EWS-FLI1 occupancy in the Ewing sarcoma cell line SK-N-MC, using BAF155 and FLI1 antibodies, respectively. The majority (95.4%) of BAF155 peaks were detected at putative enhancer regions (Figures 1D and S1F). Moreover, we

detected a striking degree of overlap between BAF155 and EWS-FLI1 sites genome-wide, for which the GGAA repeat was the top-ranked DNA motif (Figure 1E).

In addition to substantial co-localization, median BAF155 peak occupancy was 2-fold higher at EWS-FLI1-bound GGAA repeats compared to all other genomic locations (Figure 1F) and was centered on EWS-FLI1 peaks (Figures 1G–1I and S1G), suggesting that the localization of BAF complexes may be dependent on EWS-FLI1 binding. To test this hypothesis, we depleted EWS-FLI1 in SK-N-MC Ewing sarcoma cells using short hairpin RNAs (shRNAs) and found that suppression of EWS-FLI1 led to an almost complete disappearance of BAF complex occupancy at GGAA repeats (Figures 2A–2C and S2A), whereas other BAF155 peaks outside these GGAA enhancer regions remained unaffected (Figure 2D). These results were further validated by ChIP-qPCR for BAF155 occupancy over selected loci containing GGAA repeats, including *CCND1, SOX2, NR0B1,* and *LINC00221* (Figures 2E and S2B), as well as by using an antibody that recognizes the alternative BAF ATPase core subunits BRG1/BRM (Figures S2C–S2E). To account for possible effects of the cell cycle arrest observed after EWS-FLI1 knockdown (Tanaka et al., 1997), we arrested A673 cells in the G1 phase prior to performing ChIP-qPCR (Figure S2F) and co-immunoprecipitation assays (Figure S2G). Interactions and recruitment at chromatin were stable in these conditions, further confirming the specificity of decreased BAF complex occupancy at GGAA repeats observed in the absence of EWS-FLI1. These observations thus indicate that the presence of BAF complexes at GGAA repeat microsatellites is dependent on the EWS-FLI1 fusion protein.

To evaluate the potentially instructive nature of EWS-FLI1 in targeting BAF complexes, we assessed whether EWS-FLI1 is capable of site-specific recruitment of BAF complexes in MSCs, a likely cell of origin of Ewing sarcoma (Riggi et al., 2005, 2008). In this system, EWS-FLI1 has been shown to operate as a pioneer factor at GGAA repeats (Riggi et al., 2014). Whereas in naive MSCs, BAF complex occupancy over GGAA repeats was undetectable, we observed a substantial increase in BAF complex localization upon introduction of EWS-FLI1 (Figures 2F and 2G). Notably, GGAA repeats were the highest ranking DNA motif at newly created BAF complex sites, consistent with a major EWS-FLI1-mediated redistribution of BAF complexes (Figure 2H).

We next assessed whether BAF complexes are required for the induction of EWS-FLI1-mediated gene expression. shRNA-mediated depletion of the BRG1 ATPase prior to expression of EWS-FLI1 in MSCs caused a striking reduction in target gene activation (Figure 2I). Furthermore, knockdown of the subunit BAF155 in SK-N-MC Ewing sarcoma cells, using two independent BAF155-specific shRNAs, resulted in decreased expression of EWS-FLI1 target genes (Figures 2J and S2H) and significantly impaired viability of Ewing sarcoma cells in culture (Figure S2I). A similar decrease in viability was observed using shRNAs targeting the BRG1 ATPase subunit (Figure S2J). These studies performed in both MSCs and Ewing sarcoma cell lines indicate that BAF complexes play a major role in EWS-FLI1-mediated oncogenic gene regulation.

Recruitment of BAF Complexes to GGAA Repeats Is a Neomorphic Property of the EWS-FLI1 Fusion Compared to Wild-Type FLI1

The respective contributions of EWS and FLI1 components of the EWS-FLI1 fusion protein to chromatin reorganization have not to date been fully delineated. As such, we aimed to explore whether expression of the FLI1 transcription factor alone could recruit BAF complexes to GGAA repeats. In contrast to expression of EWS-FLI1, expression of the wild-type FLI1, which provides the ETS DNA binding domain to the fusion protein, did not induce de novo activation of enhancers at GGAA repeats in MSCs and was not associated with recruitment of BAF complexes (Figures 3A, 3B, and S3A). Furthermore, whereas FLI1 binding was readily detected at non-repeat canonical ETS binding motifs (Figures S3B and S3C), we did not observe significant binding for FLI1 at GGAA repeat sites (Figures 3A, 3B, and S3D). Accordingly, FLI1 failed to induce the expression of known EWS-FLI1 target genes (Figure S3E). Tethering to GGAA repeats and the recruitment of BAF complexes to these sites is thus a neomorphic property of the EWS-FLI1 fusion protein compared to wild-type FLI1.

In order to test whether these striking differences between EWS-FLI1 and wild-type FLI1 were linked to their differential ability to bind BAF complexes, we performed immunoprecipitation experiments comparing FLI1 and EWS-FLI1. Immunoprecipitation of lentivirally expressed FLI1 or EWS-FLI1 using an anti-FLI1 antibody showed that both proteins were capable of pulling down the BAF complex subunit BRG1 (Figure 3C). Consistent with these observations, further characterization showed that both the EWS N-terminal and FLI1 C-terminal fragments of EWS-FLI1 were able to co-immunoprecipitate BRG1 (Figure 3D). To test whether an additional interaction domain could account for the neomorphic properties of EWS-FLI1, we generated a fusion protein between the BAF complex subunit BAF47 and the FLI1 C-terminal domain (Figure 3E). This fusion protein was able to interact with the BAF complex, as demonstrated by immunoprecipitation (Figure 3F), and had the ability to bind and increase chromatin opening when expressed in MSCs (Figures S4A–S4D). However, in contrast to EWS-FLI1, the BAF47-FLI1 fusion protein failed to display significant binding to GGAA repeats (Figure S4E), to induce de novo enhancer formation (Figures 3G and S4F), or to activate target gene expression (Figures 3H and S4G). Thus, fusion of the FLI1 C terminus directly to the BAF chromatin remodeling complex is insufficient to replicate the pioneer function of the EWS-FLI1-bound BAF complexes at GGAA repeats, suggesting additional critical properties of the EWSR1 fragment of the fusion protein.

Fusion of EWSR1 to FLI1 Confers Prion-like Phase Transition Properties

Phase transition is defined as the ability of a biological system to undergo a change of phase or state, including transitions from protein solutions to liquid-like phase-separated compartments that constitute membrane-less organelles (Aguzzi and Altmeyer, 2016). EWSR1 belongs to the FUS, EWSR1, TAF15 (FET) family of proteins and is characterized by intrinsically disordered low-complexity prion-like domains that have been shown to mediate multimerization, physiological liquid-liquid phase separation, and pathological protein aggregation (Couthouis et al., 2011, 2012; Kato et al., 2012; Kwon et al., 2013; Schwartz et al., 2013). In keeping with these findings, we confirmed the multimerization

potential of EWSR1 by introducing GFP-tagged EWSR1 into U2OS cells and performing anti-GFP immunoprecipitation, which captured both the exogenously introduced variant (GFP-EWSR1) and endogenous EWSR1 (Figure S5A).

Given that the FET prion-like domains can undergo multimerization and concentration-dependent phase transition (Kato et al., 2012; Patel et al., 2015) and are retained in EWS-FLI1 as well as in other oncogenic fusions between FET proteins and transcription factors (Mertens et al., 2016), we first tested whether EWS-FLI1 can multimerize in the setting of Ewing sarcoma cells. In keeping with previous studies (Embree et al., 2009; Spahn et al., 2003), immunoprecipitation of tagged EWS-FLI1 showed a strong interaction with endogenous EWSR1 (Figure 4A). In contrast, tagged wild-type FLI1 only produced weak signals in these assays (Figure 4A). This suggests that a major difference between FLI1 and the fusion protein EWS-FLI1 is the ability to interact with wild-type EWSR1. In further support of this finding, immunoprecipitation followed by mass spectrometry of endogenous EWSR1 in SK-N-MC Ewing sarcoma cells, using an antibody targeting the C terminus of EWSR1 not present in EWS-FLI1, showed strong reciprocal interactions with EWS-FLI1 and also with other FETfamily proteins (TAF15 and FUS) as well as several members of the BAF complex (Figure 4B).

In order to assess the phase transition potential of EWS-FLI1, we first tested its ability to precipitate in presence of biotinylated isoxazole (b-isox), a recently identified compound with the ability to precipitate proteins with low complexity domains, including FET family proteins (Han et al., 2012; Kato et al., 2012). Our experiments show that EWS-FLI1 exhibits robust, concentration-dependent precipitation, comparable to and even higher than wild-type EWSR1 in SK-N-MC Ewing sarcoma cells (Figures 4C and 4D). This observation was recapitulated in U2OS cells stably expressing EWS-FLI1, but not in U2OS cells expressing wild-type FLI1 using the same conditions (Figure 4E).

Given that the presence of RNA has previously been shown to affect some EWSR1 interactions (Spahn et al., 2003), we tested the effects of RNase treatment in our experiments. We observed that RNase reduced b-isox-induced precipitation of EWSR1 but had small effects on EWS-FLI1 (Figure S5B). Similarly, interactions between EWS-FLI1, EWSR1, and BAF complexes (BRG1) were not significantly affected by RNase treatment (Figures S5C and S5D). These results suggest distinct properties for EWS-FLII-containing complexes and match previous in vitro results showing decreased EWSR1 homotypic interactions and stable heterotypic interactions with EWS-FLI1 upon RNase treatment (Spahn et al., 2003).

Wild-type EWSR1 has been previously shown to spontaneously precipitate in sedimentation experiments used to measure the intrinsic phase transition potential of purified proteins in vitro (Couthouis et al., 2012). We thus purified bacterially expressed glutathione S-transferase (GST)-tagged EWS-FLI1 and wild-type FLI1 to test their intrinsic phase transition potential. Sedimentation assays revealed that most EWS-FLI1 spontaneously precipitated, whereas wild-type FLI1 remained soluble in these conditions (Figures 4F, 4G, and S5E). These results demonstrate that the EWSR1 prion-like domain confers neomorphic intrinsic phase transition properties to the EWS-FLI1 oncogenic fusion protein. Supporting

these observations, confocal imaging showed that EWS-FLI1 was detectable as nuclear dot-like structures after lentiviral expression in MSCs whereas wild-type FLI1 exhibited a more diffuse pattern (Figure S5F).

Having demonstrated interactions between EWS-FLI1 and EWSR1 and similar phase transition properties conferred by their prion-like domain in vitro, we expected to find these proteins in the same complexes at GGAA repeats in Ewing sarcoma cells. To assess this, we introduced hemagglutinin (HA)-tagged EWSR1 into A673 Ewing sarcoma cells, confirmed its nuclear localization and its ability to interact with endogenous EWS-FLI1 and the BAF complex ATPase subunit BRG1 (Figures S5G and S5H), and assessed its presence at EWS-FLI1-bound GGAA microsatellite repeats. Importantly, we observed substantial co-enrichment of HA-EWSR1 and EWS-FLI1 at GGAA micro-satellite repeats, both by ChIP-seq and by validation ChIP-qPCR over selected target sites (Figures 4H–4J, S5I, and S5J). Furthermore, occupancy of HA-EWSR1 was decreased at these loci upon shRNA-mediated suppression of EWS-FLI1 (Figure S5K). Taken together, these observations suggest that EWS-FLI1 and wild-type EWSR1 are both present in the same macromolecular complexes at GGAA repeats in Ewing sarcoma.

Tyrosine Residues in the EWS-FLI1 Prion-like Domain Are Necessary for DNA Binding at GGAA Microsatellites and De Novo Enhancer Activation

We next determined whether phase transition mediated by the prion-like domain of EWS-FLI1 is necessary for DNA binding, BAF complex recruitment, and de novo enhancer activation at GGAA microsatellite repeats by generating a series of V5-tagged EWS-FLI1 mutant proteins lacking the ability to precipitate in vitro. The EWSR1 prion-like domain is rich in [G/S]Y[G/S] motifs (Figure S6A), and the substitution of these tyrosine residues with serine has been shown to abrogate phase transitions to hydrogels observed for the FET protein FUS (Kato et al., 2012; Kwon et al., 2013). Thus, we generated two EWS-FLI1 mutant proteins with point mutations altering either 12 or all 37 tyrosines in the prion-like domain (namely EWS(YS12)-FLI1 and EWS(YS37)-FLI1; Figures 5A and S6A). Both mutants were expressed and localized to the nucleus of lentivirally transduced MSCs as assessed by immunofluorescence in a manner comparable to that of EWS-FLI1 (Figures S6B and S6C). The EWS(YS12)-FLI1 mutant protein maintained significant interactions with wild-type EWSR1 and BRG1, and although diminished, b-isox-induced precipitation remained significantly higher than wild-type FLI1 (Figures 4E, 5B, and 5C). In contrast, EWS(YS37)-FLI1 displayed reduction in binding to wild-type EWSR1 and BRG1 as well as a profound loss of b-isox-induced precipitation to levels comparable to those of wild-type FLI1 (Figures 4E, 5B, and 5C). EWS(YS37)-FLI1, however, maintained the ability to homodimerize, a hallmark of ETS family transcription factors, as assessed by reciprocal immunoprecipitation experiments using overexpressed HA- and V5-tagged variants in HEK293-T cells (Figure S6D). In keeping with our results obtained with b-isox, in vitro sedimentation assays performed with purified GST-tagged EWS(YS37)-FLI1 showed a complete loss of its ability to spontaneously precipitate (Figures 5D and S6E).

Based on these findings, we further tested the ability of the EWS(YS37)-FLI1 mutant protein to bind GGAA microsatellite repeats and to create active enhancers once expressed

in MSCs (Figure S6F). ChIP-seq experiments clearly demonstrated a dramatic reduction in binding of the EWS(YS37)-FLI1 mutant at these sites, as well as impaired BAF complex recruitment (Figures5E and S6G). In line with this observation, DNA accessibility and marks of enhancer activity assessed by, respectively, ATAC-seq and ChIP-seq for H3K27ac were undetectable for the EWS(YS37)-FLI1 mutant (Figures 5E–5G, S6H, and S6I). Finally, consistent with the impairment of its biochemical properties, EWS(YS37)-FLI1 was not able to induce expression of GGAA microsatellite target genes after introduction in MSCs, whereas EWS(YS12)-FLI1 retained nearly full activity (Figure 5H). Taken together, our results demonstrate that the tyrosine residues in the EWS-FLI1 prion-like domain are necessary to mediate phase transitions and are required for its pioneer activity by allowing stable DNA binding, BAF complex recruitment at GGAA repeat microsatellites, and target gene activation.

Fusion of EWSR1 Prion-like Domain Fragments to the FLI1 C Terminus Is Sufficient to Recapitulate EWS-FLI1 Activity

Given that prion-like domains are unstructured, low-complexity protein sequences, we next tested whether any specific region within this domain is critical for EWS-FLI1 function. To this end, we generated a series of EWS-FLI1 internal deletion mutants (Figure S7A). Whereas the tyrosine residues that we showed to be critical are mostly evenly distributed over the EWSR1 prion-like domain, there are two regions that contain exact [G/S]Y[G/S] motifs followed by a glutamine (SYGQ), which we have designated as SYGQ1 (also called FETBM1; Thomsen et al., 2013) and SYGQ2. We thus deleted these regions either independently or in combination (Figure S7A). All EWS-FLI1 deletion mutant proteins accumulated in the nucleus of MSCs and exhibited comparable binding to wild-type EWSR1 and BRG1 (Figures S7B–S7D). Similarly, EWS-FLI1 deletion mutants maintained b-isox-induced precipitation properties that were diminished when compared to EWS-FLI1 but significantly higher than those of wild-type FLI1 (Figure S7E). We next assessed changes in target gene expression after introduction of the different EWS-FLI1 mutants in MSCs and observed that a large set of target genes activated by GGAA microsatellites was still strongly induced by all constructs (Figure S7F). Thus, these experiments did not identify any singular EWSR1 subdomain necessary for EWS-FLI1 activity, suggesting that there is significant functional redundancy between different parts of the EWSR1 prion-like domain.

Given these results, we tested whether small EWSR1 fragments fused to the FLI1 C-terminal region were sufficient to recapitulate EWS-FLI1 function (Figure 6A). Strikingly, the fusion of the SYGQ1 fragment (37 amino acids) was sufficient to confer binding to wild-type EWSR1 and BRG1 (Figure S7G), b-isox-induced precipitation (Figure 6B), and induction of expression of EWS-FLI1 target genes in MSCs (Figure 6C). In line with these observations, the addition of a short EWSR1 fragment was sufficient to induce precipitation of purified GST-tagged SYGQ1-FLI1 in our in vitro sedimentation assays (Figures 6D and S7H). Fusion of the SYGQ2 fragment (64 amino acids) to the FLI1 C-terminal region was also sufficient to recapitulate EWS-FLI1 function (Figures 6A–6C and S7G). In addition, a more detailed analysis of the SYGQ2 fusion showed that this mutant protein was able to bind GGAA repeat microsatellites and to recruit BAF complexes, leading to DNA

accessibility and enhancer activation, as assessed by ATAC-seq and ChIP-seq for H3K27ac, respectively (Figures 6E–6G).

Finally, the distinct abilities of mutant EWS-FLI1 proteins to recapitulate EWS-FLI1-mediated gene expression programs were evident by comparing RNA-seq expression profiles. MSCs expressing the short fragment fusion SYGQ2-FLI1 demonstrated clustering with EWS-FLI1-expressing cells (Figure 6H) whereas MSCs expressing the tyrosine mutant EWS(YS37)-FLI1 clustered with control cells infected with an empty vector (Figure 6H). In agreement with these results, cell growth arrest and phenotypic changes induced by EWS-FLI1 knockdown were rescued by the SYGQ2-FLI1 mutant protein, but not by EWS(YS37)-FLI1 (Figure S7I). These results thus demonstrate that even small isolated fragments of the EWSR1 prion-like domain are sufficient to recapitulate the function of the full EWS-FLI1 fusion on chromatin and to induce gene expression programs associated with GGAA microsatellites in Ewing sarcoma tumors.

DISCUSSION

Taken together, our studies elucidate critical mechanisms whereby EWSR1 contributes to the oncogenic activity of EWS- FLI1 (Figure 7). Low-complexity domains have been proposed to play a variety of roles in normal cellular functions and in disease states (Aguzzi and Altmeyer, 2016; March et al., 2016). In normal cells, proteins containing intrinsically disordered domains are believed to have the ability to form liquid-like compartments that, in the case of the FUS protein, have been observed in vivo in the cytoplasm upon stress and at sites of DNA damage in the nucleus (Patel et al., 2015). This process can be altered by mutations in the prion-like domain or local protein accumulation, as observed in amyotrophic lateral sclerosis (ALS), where the pathological aggregation of low-complexity proteins may be the result of the conversion from liquid to solid states (Couthouis et al., 2011, 2012; Patel et al., 2015; Sun et al., 2011). Our results suggest that a similar phase transition mechanism could allow protein accumulation and stabilization at tumor-specific DNA binding sites in Ewing sarcoma as well as in other tumor types involving fusions of FET family proteins with transcription factors. Further characterization will be necessary to pinpoint the exact nature of these transitions at chromatin. Indeed, it will be of great interest to establish whether EWS-FLI1 forms fibrils or amorphous aggregates or undergoes liquid-liquid phase separation in vivo and to what extent the disruption of these neomorphic properties may be exploited from a therapeutic standpoint.

Mutations in the genes encoding BAF complex subunits are observed in many tumor types, suggesting that tumor-specific changes in BAF complex composition and function play important roles in human cancer (Kadoch et al., 2013). We now show that, in the absence of genetic alterations in BAF complex components, the EWS-FLI1 fusion protein utilizes an alternate mechanism to retarget BAF complexes to distal regulatory elements. This, in turn, leads to the activation of target genes and the establishment of a tumor-specific regulatory network and transcriptional program. Tumor-specific retargeting of BAF complexes may thus play an important role in many tumor types in which BAF subunits are not genetically altered, thereby expanding the already wide-spanning role of these complexes in human cancer. Given our prior results showing that EWS-FLI1 also mediates the recruitment of the

acetyl-transferase P300 and mixed- lineage leukemia (MLL) complexes to GGAA repeats (Riggi et al., 2014), it will be important to determine how the interplay between these chromatin-modifying complexes leads to de novo enhancer activation.

Alterations in BAF subunits may also be associated with changes in both subunit composition and configuration of the BAF complex. This has been demonstrated in synovial sarcoma, where the SS18-SSX translocation leads to the formation of a modified version of the BAF complex that incorporates the translocation protein (Kadoch and Crabtree, 2013). Our results show that, despite strong interactions with BAF, EWS-FLI1 is not incorporated into the core BAF complex and therefore does not affect BAF composition directly. Nevertheless, the recruitment of BAF complexes to GGAA repeats in association with the potential phase transitions induced by the EWSR1 prion-like motif may involve an unusual configuration that could be exploited for the development of new therapeutic approaches.

Our experiments comparing EWS-FLI1, FLI1, and various mutant proteins in MSCs establish a direct link between the neomorphic properties conferred by the EWS prion-like domain and a tumor-specific gene regulation program mediated by de novo enhancer activation at GGAA microsatellites. Indeed, FLI1 exhibited substantial occupancy at canonical ETS binding sites but, in contrast to EWS-FLI1, was not able to bind GGAA repeats. This is in agreement with the observation that Ewing sarcoma cell lines were the only cell types with open chromatin at EWS-FLI1-bound GGAA microsatellite repeats in a survey of 112 cell types analyzed by DNase hypersensitivity (Riggi et al., 2014). These data included profiles for cells that express high levels of endogenous FLI1 and yet did not show signals at GGAA repeat sites. This is also consistent with recent studies suggesting that various types of stem cells may contain destabilized nucleosomes detected by FAIRE (formaldehyde-assisted isolation of regulatory elements) at repetitive elements, but not open chromatin (Gomez et al., 2016). Importantly, prior electro-phoretic mobility shift (EMSA) assays showed binding of both EWS-FLI1 and FLI1 to GGAA repeats in vitro (Gangwal et al., 2008), suggesting that the difference between these two proteins may only be evident in the appropriate in vivo chromatin context. The application of methods for direct high-throughput genome-wide analysis of chromatin thus provides opportunities for new insights into critical mechanisms of oncogenic gene regulation.

In conclusion, our study demonstrates that a prion-like domain can confer neomorphic properties to fusion proteins that lead to retargeting of key chromatin regulators and the establishment of an oncogenic gene regulatory program. Similar events mediated by FET family proteins or other intrinsically disordered proteins are likely to play important roles in generating tumor-specific regulatory elements in a variety of tumor types and may constitute attractive targets for therapeutic development.

STAR★METHODS

CONTACT FOR REAGENT AND RESOURCE SHARING

Further information and requests for resources and reagents should be directed to and will be fulfilled by Lead Contact Miguel N. Rivera (mnrivera@mgh.harvard.edu).

EXPERIMENTAL MODEL AND SUBJECT DETAILS

Mesenchymal stem cells—Mesenchymal stem cells were collected with approval from the Institutional Review Board of the Centre Hospitalier Universitaire Vau- dois (CHUV, University of Lausanne). Samples were deidentified prior to our analysis. Primary bone marrow derived mesenchymal stem cells were cultured in Iscove's modified Dulbecco's medium containing 10% fetal calf serum (FCS) and 10 ng/ml platelet-derived growth factor BB (PeproTech).

Cell lines—Cell lines were obtained from ATCC and media from Life Technologies. Ewing sarcoma cell lines SKNMC and A673 were grown in RPMI. HEK293-T, U2OS, and SAOS2 cells were grown in DMEM. All media were supplemented with 10% FBS and cells were cultured at 37°C with 5% CO2. Cells were maintained and split every 2–3 days according to ATCC recommendations.

Bacterial Cultures—For protein production, *E. coli* BL21 (DE3) pLysS (Fisher Scientific) were grown in LB medium supplemented with 100 μg/ml ampicillin and 25 μg/ml chloramphenicol. At absorbance A600 = 0.8, protein expression in *E. coli* cultures was induced by adding 0.1 mM IPTG and incubated overnight at 16°C with agitation.

METHOD DETAILS

Lentiviral Generation—Lentivirus was produced in 293T LentiX cells (Clontech) either by polyethylenimine (PEI) (Polysciences) transfection with gene delivery vector and packaging vectors pspax2 and pMD2.G (Kadoch and Crabtree, 2013) or by LT1 (Mirus Bio) transfection with gene delivery vector and packaging vectors GAG/POL and VSV plasmids (Boulay et al., 2017). Viral supernatants were collected 72h after transfection and concentrated using either ultracentrifugation (2 hr+4°C at 20,000 rpm) or LentiX concentrator (Clontech). Virus containing pellets were resuspended in PBS and added dropwise on cells in presence of media supplemented with 6 μg/ml polybrene. Selection of lentivirally-infected cells was achieved with puromycin used at 0.75–1-2 μg/ml (MSC, SK-N-MC and A673/U2OS respectively) and blasticidin used at 7 μg/ml in MSC and U2OS. Overexpression or knockdown efficiency was determined by western blot analysis and RT-qPCR.

Transient Transfections—HEK293T cells were plated to 80% confluency prior to transfection using LT1 (Mirus Bio) or PEI (Polysciences) according to the manufacturer recommendations and were collected after 48h.

Real-Time Quantitative RT-PCR—For gene expression assays, total RNA was isolated from cells using NucleoSpin RNA Plus (Clontech). cDNA was obtained using a high-capacity RNA to-cDNA kit (Applied Biosystems). 500 nanograms of template total RNA and random hexamers were used for each reaction. Real-time PCR amplification was performed using fast SYBR Green Master Mix (Life Technologies) and specific PCR primers in a Lightcycler 480 instrument (Roche). Oligonucleotides used are provided in Table S1. Relative quantification of each target, normalized to an endogenous control (GAPDH or HPRT1), was performed using the comparative Ct method (Applied

Biosystems). Error bars indicate SD of three technical replicates and represent at least two independent biological experiments. Statistical analyses were performed by Student's t test. In heatmaps, log2 qRT-PCR expression values were averaged across biological replicates in each condition and scaled for each gene.

Western Blot Analysis—Western blotting was performed using standard protocols. Primary antibodies used for western blotting are listed in Table S1. Secondary antibodies were goat anti-rabbit and goat anti-mouse immunoglobulin G-horseradish peroxidase-conjugated (BioRad, 1:10,000 dilution). Membranes were developed using Western Lightning Plus-ECL enhanced chemiluminescence substrate (PerkinElmer) and visualized using photographic film. Alternatively, IRDye (Li-COR Biosciences, Lincoln, NE, USA) secondary antibodies were used for visualization with the Li-Cor Oddessy Imaging System (Li-COR Biosciences, Lincoln, NE, USA).

Nuclear Extract Preparation—Cells were homogenized in Buffer A (25 mM HEPES (pH 7.6), 25 mM KCL, 0.05 mM EDTA, 10% glycerol, 5mM MgCl2, 0.1% NP-40, supplemented with fresh 1mM DTT, protease inhibitors [Roche], and 1mM PMSF) on ice. Nuclei were sedimented by centrifugation (1,200 rpm), resuspended in Buffer C (10 mM HEPES (pH 7.6), 3 mM MgCl2, 100 mM KCL, 0.1 mM EDTA, 10% glycerol, 1 mM DTT and protease inhibitors), and lysed by the addition of ammonium sulfate to a final concentration of 300 mg/mL. Soluble nuclear proteins were separated by ultracentrifugation (100,000 x g) and precipitated with 0.3 mg/ml ammonium sulfate for 20 min on ice. Protein precipitate was isolated by ultracentrifugation (100,000 x g) and resuspended in IP buffer 1 (300 mM NaCl, 25 mM HEPES [pH 8.0], 0.1% Tween-20,10% Glycerol, 1 mM DTT, 1 mM PMSF with protease inhibitors) or IP buffer 2 (150 mM NaCl, 50 mM Tris-HCl, 1 mM EDTA, 1% Triton X-100,1 mM DTT, 1 mM PMSF with protease inhibitors) for immunoprecipitation analyses or HEMG-0 buffer (25 mM HEPES [pH 7.9], 0.1 mM EDTA, 12.5 mM MgCl2,100 mM KCl, supplemented with DTT and PMSF) for analyses on glycerol gradient.

Immunoprecipitations—Nuclear extracts were resuspended in IP buffer and placed in protein lo-bind tubes (Eppendorf). Protein concentration was determined using Bradford assay and adjusted to the final volume of 200 µL at a final concentration of 1 mg/ml with IP buffer. Each IP was incubated with 2 µg of antibody (Antibody specifications are found in Table S1) overnight at 4°C and then for 1h with 20 µL Protein G Dynabeads (Life Technologies) or Protein G Sepharose beads (GE Heathcare). The beads were then washed five times at 4°C with IP buffer and resuspended in 20 µL 2x gel loading buffer (4x LDS buffer; Invitrogen) + DTT and water.

Alternatively, immunoprecipitations were performed as previously described (Boulay et al., 2017): cells were resuspended in IPH Buffer (50 mM Tris-HCl pH 8,150 mM NaCl, 5 mM EDTA, 0.5% NP-40 and 10% glycerol supplemented with protease and phosphatase inhibitors (Pierce) and 1mM PMSF) before sonication in a QSONICA 800 R instrument. Protein supernatant was then collected after centrifugation for 15 min at 14 000 rpm and 4°C. Proteins were quantified using a Bradford assay (Pierce) and 500 µg of lysate were diluted in IPH buffer to a final volume of 1 mLand incubated overnight at +4°C with 2 µg of

the indicated antibodies in the presence of magnetic G-Dynabeads (Life Technologies) and 100 μg/mL Ethidium Bromide (SIGMA-ALDRICH). 100 μg/mL RNase A (Life Technologies) was used for RNase treatment experiments. Beads were washed 5 times with IPH buffer and eluted by boiling in loading Laemmli buffer.

Depletion Studies—Nuclear extracts were prepared to a final concentration of 2.5 mg/ml with IP buffer 2. For each IP, 75ug (30 μL) of nuclear extract was incubated with 2.5 μg of antibody overnight at 4°C and then for 1h with 15 μL pre-washed Protein G Sepharose beads. After centri-fugation (10,000 rpm for 1min) 45 μL of the supernatant was either saved or used for another round of IP. In total 3 rounds of IP were performed. Quantitative densitometry analyses were performed with the Li-Cor Oddessy Imaging System (Li-COR Biosciences, Lincoln, NE, USA).

Urea Denaturation Studies—Nuclear extracts (150 μg) were subjected to partial urea denaturation, ranging from 0.25 to 2.5 M urea (in IP buffer), for 30 min at room temperature (RT) prior to anti-EWSR1 IP. The co-precipitated proteins were analyzed by immunoblot.

Density Sedimentation Analyses—Nuclear extracts (500 mg) were resuspended in 200 μL of 0% glycerol HEMG buffer and carefully overlaid onto a 10 mL 10%−30% glycerol (in HEMG buffer) gradient prepared in a 14 3 89 mm polyallomer centrifuge tube (331327, Beckman Coulter, Brea, CA, USA). Tubes were centrifuged in an SW40 rotor at 4°C for 16 hr at 40,000 rpm. Fractions (0.5 mL) were collected and used in analyses.

Mass Spectrometry—Immunoprecipitation using either IgG (Cell Signaling Technology) or anti-EWSR1 (Bethyl) crosslinked antibodies was performed in SK-N-MC nuclear extracts. Immunoprecipitation samples were then run on a4%−12% Bis-Tris Gel (Thermo Scientific) and subjected to Coomassie staining. Bands were then cut from each IP and submitted totheTaplin Biological Mass Spectrometry Facility (Harvard Medical School) for analysis.

ChIP-seq—ChIP assays were carried out on A673, SKNMC and MSCs cultures of approximately 2–5 million cells per sample and per epitope, following the procedures described previously (Mikkelsen et al., 2007). In brief, chromatin from formaldehyde-fixed cells was fragmented to a size range of 200–700 bases with a Branson 250 sonifier. Solubilized chromatin was immunoprecipitated with the indicated antibodies overnight at 4°C. Antibody-chromatin complexes were pulled down with protein G-Dynabeads (Life Technologies), washed, and then eluted. After crosslink reversal, RNaseA, and proteinase K treatment, immunoprecipitated DNA was extracted with AMP Pure beads (Beckman Coulter). ChIP DNA was quantified with Qubit. 1–5 ng ChIP DNA samples were used to prepare sequencing libraries, and ChIP DNA and input controls were sequenced with the Nextseq 500 Illumina genome analyzer.

ChIP-seq Bioinformatic Analysis—Reads were aligned to hg19 using bwa (Li and Durbin, 2009). Aligned reads were then filtered to exclude PCR duplicates and were extended to 200 bp to approximate fragment sizes. Density maps were generated by counting the number of fragments overlapping each position using igvtools, and normalized

to 10 million reads. We used MACS2 (Zhang et al., 2008) to call peaks using matching input controls with a q-value threshold of 0.01. BAF155 peaks were called using the-broad parameter and were considered promoter peaks if they were within 1 kb of transcriptional start sites (TSSs) in the Refseq database. Peaks were filtered to exclude blacklisted regions as defined by the ENCODE consortium (Consortium, 2012). Peaks within 200 bp of each other were merged. Peak intersections were identified using bedtools (Quinlan and Hall, 2010). Average ChIP-seq signals across intervals were calculated using bwtool (Pohl and Beato, 2014). Total ChIP-seq signals were calculated by multiplying average signals by peak length. For motif discovery and peak annotations, we used Homer suite of tools (Heinz et al., 2010). findMotifsGenome.pl was used to identify de novo motifs within 500 bp flanking centers of distal peaks.TheannotatePeaks.pl script was used to assign peaks to annotations. Signals shown in heatmaps (100 bp windows) and composite plots (10 bp window) were calculated using bwtool (Pohl and Beato, 2014). Heatmap signals are in log2 scale, centered around EWS-FLI1-bound GGAA repeat enhancers previously described (Riggi et al., 2014) (N = 812) and are capped at the 99th percentile.

ChIP-qPCR—Chromatin immunoprecipitation was performed as descrived above. Quantitative PCR was performed using fast SYBR Green Master Mix (Life Technologies) and specific PCR primers in a Lightcycler 480 instrument (Roche). Oligonucleotides used are provided in Table S1. Relative quantification of each target, normalized to INPUT control, was performed using the comparative Ct method (Applied Biosystems). Error bars indicate SD of three technical replicates and represent at least two independent biological experiments.

RNA-Seq—Total RNA was isolated from cells using NucleoSpin RNA Plus (Clontech). 0.5–1 ug of total RNA was treated with Ribogold zero to remove ribosomal RNA. Illumina sequencing libraries were constructed using random primers according to the manufacturer's instructions using the Truseq Stranded RNA LT Kit.

RNA-seq bioinformatic Processing—Reads were aligned to hg19 using STAR (Dobin et al., 2013). Mapped reads were filtered to exclude PCR duplicates and reads mapping to known ribosomal RNA coordinates, obtained from rmsk table in the UCSC database (http://genome.ucsc.edu). Gene expression was calculated using featureCounts (Liao et al., 2014). Only primary alignments with mapping quality of 10 or more were counted. Counts were then normalized to 1 million reads. Signal tracks were generated using bedtools (Quinlan and Hall, 2010). Differential expression was calculated using DESeq2 (Love et al., 2014).

Definition of target genes associated with EWS-FLI1 bound GGAA-repeats—To compare changes in expression of GGAA-repeat associated EWS-FLI1 target genes in MSC experiments, we selected genes based on downregulation upon EWS-FLI1 knockdown in both A673 and SKNMC Ewing sarcoma cells (greater than 2-fold) and a maximum distance of 1 megabase from a EWS-FLI1-bound GGAA repeat (Riggi et al., 2014). Genes were included in heatmaps if they were significantly upregulated (2 fold change and corrected p value < 0.05) in the positive control EWS-FLI1 infection in a given experiment.

Normalized expression values were averaged across biological replicates in each condition and scaled for each gene.

Principal Component Analysis—Principal Component Analysis (PCA) was performed using the R package "prcomp." Principal components were calculated separately for repeat-associated genes (as described above) and non-repeat-associated genes with reciprocal changes in EWS-FLI1 knockdowns (2-fold in A673 and SKNMC cells) and MSCs infected with EWS-FLI1 (2-fold and corrected p value <0.05). PC rotations obtained by evaluating MSCs infected with EWS-FLI1 and controls were used to calculate PC1 scores for other conditions.

ATAC-seq Genome-Wide DNA Accessibility Assay—ATAC-seq analysis on human pediatric MSCs was performed as recently described (Buenrostro et al., 2013). Briefly, 5×10^4 cells for each condition were first incubated in hypotonic buffer then resuspended in lysis buffer, centrifugated and resuspended in Transposase reaction mix for additional 30 min at 37°C, following manufacturer recommendations (Nextera DNA sample Prep Kit, Illumina). After DNA purification, adaptor sequences were added to the fragmented DNA by PCR. Purified PCR products were sequenced using the Illumina Nextseq device.

ATAC-seq bioinformatic Processing—Paired end reads were aligned to hg19 using bwa (Li and Durbin, 2009). Reads that aligned in the proper orientation and on the same chromosome were then filtered to exclude PCR duplicates and processed as previously described (Buenrostro et al., 2013). Briefly, read start sites were adjusted to represent the center of the transposon binding event (+4 bp in the plus strand and −5 bp in the minus strand). Signal densities were calculated over a sliding 150 bp window at 20 bp steps and normalized to 10 million reads in each experiment using bedtools (Quinlan and Hall, 2010). Average ATAC-seq signals across intervals was calculated using bwtool (Pohl and Beato, 2014). To test chromatin opening in non-GGAA repeat sites after BAF47-FLI1 expression, ATAC-seq signals were measured at the top 10,000 new peaks detected with the FLI1 antibody after introduction of BAF47-FLI1.

Immunofluorescence Stainings—Staining was performed using standard protocols. Briefly, cells were fixed in a 1X PBS solution containing 4% paraformaldehyde 15 min at room temperature (RT), washed with 1X PBS and stored at 4°C. Cells were permeabilized 10 min at RTin 1XPBS containing 0.5% Triton X-100 then blocked for 30 min at RT, stained with the relevant antibody for 2 hr at RT and with Alexa Fluor 546-conjugated secondary antibody (Life Technologies) for 1h at RT in the dark. Cells were washed with 1X PBS between each step of the protocol. Nuclei were stained with DAPI solution.

Cell Viability Assays—Cells were seeded in triplicates and grown under log phase growth conditions in cell culture treated 96 well plate. After the indicated incubation times, cell viability was measured using the CellTiter-Glo luminescent assay (Promega) as described by the manufacturer. Endpoint luminescence was measured on a SpectraMax M5 plate reader (Molecular Devices). The data displayed are representative of at least two biological experiments. Statistical analyses were performed by Student's t test.

G1 Arrest Experiments—A673 cells were treated with Palbociclib (PD 0332991 ISETHIONATE, Sigma-Aldrich) at a final concentration of 1.5 uM for 24 hr.

Biotinylated isoxazole-Mediated Precipitation—These assays were performed as previously described (Kato et al., 2012) with slight modifications. Biotinylated isoxazole (b-isox, Sigma-Aldrich) was reconstituted in DMSO. Briefly, 5–10 million cells were resuspended in 1 mL lysis buffer (20 mM Tris-HCl pH 7.4, 150 mM NaCl, 5 mM MgCl2, 0.5% NP-40 and 10% glycerol supplemented with 1X Protease/Phosphatase inhibitors (Pierce), 0.1 mM PMSF and 20 mM beta-mercaptoethanol) and incubated for 30 min with rotation at +4°C. Protein supernatant was then collected after centrifugation for 15 min at 14000 rpm +4°C. A 5% whole cell extract (WCE) control was collected and the remaining proteins were divided into four aliquots before addition of biotinylated isoxazole at 0,10, 30 100 uM final concentrations. 100 μg/mL RNase A (Life Technologies) was used for RNase treatment experiments. The Reaction solutions were incubated at +4°C for 1h with rotation and centrifuged for 15 min at 14000 rpm +4°C. Supernatant was saved for further analysis and pellets were washed twice in supplemented Lysis buffer before resuspension in Laemmli buffer. WCE, pellets and supernatants were analyzed by 4%−12% Tris-Glycine gradient gels (Life Technologies) and western blotting was performed using standard protocols.

Protein purification and sedimentation assays—Recombinant proteins were purified as previously described (Couthouis et al., 2011; Sun et al., 2011) with minor modifications. Wild-type and mutant constructs were cloned in pGEX-6P1, and expressed in *E. coli* BL21 (DE3) pLysS (Fisher Scientific). Bacteria were grown in LB medium supplemented with 100 μg/ml ampicillin and 25 μg/ml chloramphenicol. At absorbance A600 = 0.8, protein expression in *E. coli* cultures was induced by adding 0.1 mM IPTG and incubated overnight at 16°C with agitation. Cells were harvested by centrifugation and cell pellets were resuspended in 40 mL GST buffer (1X PBS, 150 mM NaCl, 1.5 mM EDTA, 1mM DTT, 0.2% Triton X-100 and Protease/phosphatase inhibitors (Sigma)). The homogenized suspension was sonicated 3 times on ice for 30 s. The insoluble materials were removed by centrifugation (15,000 rpm 20 min at 4°C) and the clarified supernatants were incubated with glutathione Sepharose beads (GE Healthcare) or glutathione magnetic agarose beads (Pierce) for 2 hr at 4°C. The beads were washed 3 times with GST washing buffer (1X PBS, 350 mM NaCl, 1mM EDTA, and 1mM DTT) and once with equilibration buffer (50 mM Tris-HCl pH 8,100 mM KAc, 200 mM trehalose, 0.5 mM EDTA). Recombinant proteins were eluted with GST elution buffer (50 mM Tris-HCl pH 8,100 mM KAc, 200 mM trehalose, 0.5 mM EDTA, 20 mM glutathione) for 2h at 4°C. Eluted proteins were centrifuged (16,000 g 10 min at 4°C) prior to quantification by Bradford assay. Recombinant proteins (2.5 μM) were then resuspended in reaction buffer (50 mM Tris-HCl, pH 8,100 mM potassium acetate, 200 mM trehalose, 0.5 mM EDTA, 20 mM glutathione, 60 U/mL Scission Protease) and incubated at 25°C for 60 min with agitation (1,200 rpm) in an Eppendorf Thermomixer before centrifugation at 16,000 g for 10 min at +25°C. Recombinant GST-EWS-FLI1 bound to magnetic beads was quantified against a bovine serum albumin standard dilution by SDS-PAGE and Coomassie staining and magnetic beads were removed before final centrifugation. Supernatant and pellet fractions were then resolved by SDS-PAGE and stained with Coomassie Blue. The amount in either fraction was

determined by densitometry in comparison to an input reaction control using ImageJ software.

QUANTIFICATION AND STATISTICAL ANALYSES

All statistical details of experiments are included in the Figure legends or specific Methods section.

DATA AND SOFTWARE AVAILABILITY

The data accompanying this paper have been deposited into GEO under accession number GSE94278.

ADDITIONAL RESOURCES

To aid our analysis, we also used our publicly available dataset for EWS-FLI1 and H3K27ac ChIP-seq in A673 and SK-N-MC cells (GEO: GSE61953) (Riggi et al., 2014).

Supplementary Material

Refer to Web version on PubMed Central for supplementary material.

ACKNOWLEDGMENTS

We thank S. Gillepsie, M. Bobbin, M. Aryee, and N. Mashtalir as well as members of the Rivera, Kadoch, Bernstein, and Suva labs for valuable guidance and advice. We thank L. Nieman of the MGH Cancer Center/Molecular Pathology Confocal Core (MGH) and members of the Taplin Mass Spec Facility (HMS) for assistance with experiments and data analysis. We thank G.R. Crabtree and A. Kuo for kindly sharing the homemade BAF155 (SMARCC1) antibody used in ChIP-seq experiments. G.J.S. is supported by the Department of Defense Prostate Cancer Research Program Postdoctoral Training Award W81XWH-15–1-0659. N.R. is supported by the Swiss National Science Foundation Professorship grant (PP00P3–157468/1) and the MEDIC Foundation. R.B. is supported by a NIH Pathway to Independence Award (1K99CA212154). C.K. is supported by the NIH DP2 New Innovator Award 1DP2CA195762–01, the American Cancer Society Research Scholar Award RSG-14–051-01-DMC, and the Pew-Stewart Scholars in Cancer Research Grant. This work was also supported by the Alex's Lemonade Stand Foundation Young Investigator Award (C.K.). M.N.R. is supported by the V Foundation for Cancer Research. M.N.R. is a consultant for Loxo and receives research support from Affymetrix. C.K. is a scientific founder, shareholder, and consultant for Foghorn Therapeutics.

REFERENCES

Aguzzi A, and Altmeyer M. (2016). Phase separation: linking cellular compartmentalization to disease. Trends Cell Biol. 26, 547–558. [PubMed: 27051975]

Boulay G, Awad ME, Riggi N, Archer TC, Iyer S, Boonseng WE, Rossetti NE, Naigles B, Rengarajan S, Volorio A, et al. (2017). OTX2 activity at distal regulatory elements shapes the chromatin landscape of group 3 medulloblastoma. Cancer Discov. 7, 288–301. [PubMed: 28213356]

Brohl AS, Solomon DA, Chang W, Wang J, Song Y, Sindiri S, Patidar R, Hurd L, Chen L, Shern JF, et al. (2014). The genomic landscape of the Ewing sarcoma family of tumors reveals recurrent STAG2 mutation. PLoS Genet. 10, e1004475.

Buenrostro JD, Giresi PG, Zaba LC, Chang HY, and Greenleaf WJ (2013). Transposition of native chromatin for fast and sensitive epigenomic profiling of open chromatin, DNA-binding proteins and nucleosome position. Nat. Methods 10, 1213–1218. [PubMed: 24097267]

Couthouis J, Hart MP, Shorter J, DeJesus-Hernandez M, Erion R, Oristano R, Liu AX, Ramos D, Jethava N, Hosangadi D, et al. (2011).A yeast functional screen predicts new candidate ALS disease genes. Proc. Natl. Acad. Sci. USA 108, 20881–20890. [PubMed: 22065782]

Couthouis J, Hart MP, Erion R, King OD, Diaz Z, Nakaya T, Ibrahim F, Kim HJ, Mojsilovic-Petrovic J, Panossian S, et al. (2012). Evaluating the role of the FUS/TLS-related gene EWSR1 in amyotrophic lateral sclerosis. Hum. Mol. Genet 21, 2899–2911. [PubMed: 22454397]

Crompton BD, Stewart C, Taylor-Weiner A, Alexe G, Kurek KC, Calicchio ML, Kiezun A, Carter SL, Shukla SA, Mehta SS, et al. (2014). The genomic landscape of pediatric Ewing sarcoma. Cancer Discov. 4, 1326–1341. [PubMed: 25186949]

Delattre O, Zucman J, Plougastel B, Desmaze C, Melot T, Peter M, Kovar H, Joubert I, de Jong P, Rouleau G, et al. (1992). Gene fusion with an ETS DNA-binding domain caused by chromosome translocation in human tumours. Nature 359, 162–165. [PubMed: 1522903]

Dobin A, Davis CA, Schlesinger F, Drenkow J, Zaleski C, Jha S, Batut P, Chaisson M, and Gingeras TR (2013). STAR: ultrafast universal RNA-seq aligner. Bioinformatics 29, 15–21. [PubMed: 23104886]

Embree LJ, Azuma M, and Hickstein DD (2009). Ewing sarcoma fusion protein EWSR1/FLI1 interactswith EWSR1 leading to mitotic defects in zebra- fish embryos and human cell lines. Cancer Res. 69, 4363–4371. [PubMed: 19417137]

ENCODE Project Consortium (2012). An integrated encyclopedia of DNA elements in the human genome. Nature 489, 57–74. [PubMed: 22955616]

Gangwal K, Sankar S, Hollenhorst PC, Kinsey M, Haroldsen SC, Shah AA, Boucher KM, Watkins WS, Jorde LB, Graves BJ, and Lessnick SL (2008). Microsatellites as EWS/FLI response elements in Ewing's sarcoma. Proc. Natl. Acad. Sci. USA 105, 10149–10154. [PubMed: 18626011]

Gomez NC, Hepperla AJ, Dumitru R, Simon JM, Fang F, and Davis IJ (2016). Widespread chromatin accessibility at repetitive elements links stem cells with human cancer. Cell Rep. 17, 1607–1620. [PubMed: 27806299]

Guillon N, Tirode F, Boeva V, Zynovyev A, Barillot E, and Delattre O. (2009). The oncogenic EWS-FLI1 protein binds in vivo GGAA microsatellite sequences with potential transcriptional activation function. PLoS ONE 4, e4932.

Han TW, Kato M, Xie S, Wu LC, Mirzaei H, Pei J, Chen M, Xie Y, Allen J, Xiao G, and McKnight SL (2012). Cell-free formation of RNA granules: bound RNAs identify features and components of cellular assemblies. Cell 149, 768–779. [PubMed: 22579282]

Heinz S, Benner C, Spann N, Bertolino E, Lin YC, Laslo P, Cheng JX, Murre C, Singh H, and Glass CK (2010). Simple combinations of lineage-determining transcription factors prime cis-regulatory elements required for macrophage and B cell identities. Mol. Cell 38, 576–589. [PubMed: 20513432]

Herrero-Martin D, Fourtouna A, Niedan S, Riedmann LT, Schwentner R, and Aryee DN (2011). Factors affecting EWS-FLI1 activity in Ewing's sarcoma. Sarcoma 2011, 352580.

Kadoch C, and Crabtree GR (2013). Reversible disruption of mSWI/SNF (BAF) complexes by the SS18-SSX oncogenic fusion in synovial sarcoma. Cell 153,71–85. [PubMed: 23540691]

Kadoch C, and Crabtree GR (2015). Mammalian SWI/SNF chromatin remodeling complexes and cancer: Mechanistic insights gained from human genomics. Sci. Adv 1, e1500447.

Kadoch C, Hargreaves DC, Hodges C, Elias L, Ho L, Ranish J, and Crabtree GR (2013). Proteomic and bioinformatic analysis of mammalian SWI/SNF complexes identifies extensive roles in human malignancy. Nat. Genet 45, 592–601. [PubMed: 23644491]

Kato M, Han TW, Xie S, Shi K, Du X, Wu LC, Mirzaei H, Goldsmith EJ, Longgood J, Pei J, et al. (2012). Cell-free formation of RNA granules: low complexity sequence domains form dynamic fibers within hydrogels. Cell 149, 753–767. [PubMed: 22579281]

Kovar H. (2011). Dr. Jekyll and Mr. Hyde: the two faces of the FUS/EWS/ TAF15 protein family. Sarcoma 2011, 837474.

Kwon I, Kato M, Xiang S, Wu L, Theodoropoulos P, Mirzaei H, Han T, Xie S, Corden JL, and McKnight SL (2013). Phosphorylation-regulated binding of RNA polymerase II to fibrous polymers of low-complexity domains. Cell 155, 1049–1060. [PubMed: 24267890]

Lander ES (2011). Initial impact of the sequencing of the human genome. Nature 470, 187–197. [PubMed: 21307931]

Lawrence MS, Stojanov P, Polak P, Kryukov GV, Cibulskis K, Siva-chenko A, Carter SL, Stewart C, Mermel CH, Roberts SA, et al. (2013). Mutational heterogeneity in cancer and the search for new cancer- associated genes. Nature 499, 214–218. [PubMed: 23770567]

Li H, and Durbin R. (2009). Fast and accurate short read alignment with Burrows-Wheeler transform. Bioinformatics 25, 1754–1760. [PubMed: 19451168]

Liao Y, Smyth GK, and Shi W. (2014). featureCounts: an efficient general purpose program for assigning sequence reads to genomic features. Bioinformatics 30, 923–930. [PubMed: 24227677]

Love MI, Huber W, and Anders S. (2014). Moderated estimation of fold change and dispersion for RNA-seq data with DESeq2. Genome Biol. 15, 550. [PubMed: 25516281]

March ZM, King OD, and Shorter J. (2016). Prion-like domains as epigenetic regulators, scaffoldsforsubcellularorganization, and drivers ofneurode- generative disease. Brain Res. 1647, 9–18. [PubMed: 26996412]

Mertens F, Antonescu CR, and Mitelman F. (2016). Gene fusions in soft tissue tumors: Recurrent and overlapping pathogenetic themes. Genes Chromosomes Cancer 55,291–310. [PubMed: 26684580]

Mikkelsen TS, Ku M, Jaffe DB, Issac B, Lieberman E, Giannoukos G, Alvarez P, Brockman W, Kim TK, Koche RP, et al. (2007). Genome-wide maps of chromatin state in pluripotent and lineage-committed cells. Nature 448, 553–560. [PubMed: 17603471]

Patel M, Simon JM, Iglesia MD, Wu SB, McFadden AW, Lieb JD, and Davis IJ (2012).Tumor-specific retargeting of an oncogenic transcription factor chimera results in dysregulation of chromatin and transcription. Genome Res. 22, 259–270. [PubMed: 22086061]

Patel A, Lee HO, Jawerth L, Maharana S, Jahnel M, Hein MY, Stoynov S, Mahamid J, Saha S, Franzmann TM, et al. (2015). A liquid-to-solid phase transition ofthe ALS protein FUS accelerated by disease mutation. Cell 162,1066–1077. [PubMed: 26317470]

Phelan ML, Sif S, Narlikar GJ, and Kingston RE (1999). Reconstitution of a core chromatin remodeling complex from SWI/SNF subunits. Mol. Cell 3, 247–253. [PubMed: 10078207]

Pohl A, and Beato M. (2014). bwtool: a tool for bigWig files. Bioinformatics 30, 1618–1619. [PubMed: 24489365]

Quinlan AR, and Hall IM (2010). BEDTools: a flexible suite of utilities for comparing genomic features. Bioinformatics 26, 841–842. [PubMed: 20110278]

Riggi N, Cironi L, Provero P, Suva ML, Kaloulis K, Garcia-Echeverria C, Hoffmann F, Trumpp A, and Stamenkovic I. (2005). Development of Ewing's sarcoma from primary bone marrow-derived mesenchymal progenitor cells. Cancer Res. 65, 11459–11468. [PubMed: 16357154]

Riggi N, Suvà ML, Suvà D, Cironi L, Provero P,Tercier S, Joseph JM, Stehle JC, Baumer K, Kindler V, and Stamenkovic I. (2008). EWS-FLI-1 expression triggers a Ewing's sarcoma initiation program in primary human mesenchymal stem cells. Cancer Res. 68, 2176–2185. [PubMed: 18381423]

Riggi N, Knoechel B, Gillespie SM, Rheinbay E, Boulay G, Suvà ML, Rossetti NE, Boonseng WE, Oksuz O, Cook EB, et al. (2014). EWS- FLI1 utilizes divergent chromatin remodeling mechanisms to directly activate or repress enhancer elements in Ewing sarcoma. Cancer Cell 26, 668–681. [PubMed: 25453903]

Roberts CW, Leroux MM, Fleming MD, and Orkin SH (2002). Highly penetrant, rapid tumorigenesis through conditional inversion of the tumor suppressor gene Snf5. Cancer Cell 2, 415–425. [PubMed: 12450796]

Schwartz JC, Wang X, Podell ER, and Cech TR (2013). RNA seeds higher-order assembly of FUS protein. Cell Rep. 5, 918–925. [PubMed: 24268778]

Spahn L, Siligan C, Bachmaier R, Schmid JA, Aryee DN, and Kovar H. (2003). Homotypic and heterotypic interactions of EWS, FLI1 and their oncogenic fusion protein. Oncogene 22, 6819–6829. [PubMed: 14534527]

Sun Z, Diaz Z, Fang X, Hart MP, Chesi A, Shorter J, and Gitler AD (2011). Molecular determinants and genetic modifiers of aggregation and toxicity for the ALS disease protein FUS/TLS. PLoS Biol. 9, e1000614.

Tanaka K, Iwakuma T, Harimaya K, Sato H, and Iwamoto Y. (1997). EWS-Fli1 antisense oligodeoxynucleotide inhibits proliferation of human Ewing's sarcoma and primitive neuroectodermal tumor cells. J. Clin. Invest 99, 239–247. [PubMed: 9005992]

Thomsen C, Grundevik P, Elias P, Stahlberg A, and Aman P. (2013). A conserved N-terminal motif is required for complex formation between FUS, EWSR1, TAF15 and their oncogenic fusion proteins. FASEB J. 27, 4965–4974. [PubMed: 23975937]

Tirode F, Surdez D, Ma X, Parker M, Le Deley MC, Bahrami A, Zhang Z, Lapouble E, Grossetete-Lalami S, Rusch M, et al.; St. Jude Children's Research Hospital-Washington University Pediatric Cancer Genome Project and the International Cancer Genome Consortium (2014). Genomic landscape of Ewing sarcoma defines an aggressive subtype with co-association of STAG2 and TP53 mutations. Cancer Discov. 4, 1342–1353. [PubMed: 25223734]

Tomazou EM, Sheffield NC, Schmidl C, Schuster M, Schönegger A, Datlinger P, Kubicek S, Bock C, and Kovar H. (2015). Epigenome mapping reveals distinct modes of gene regulation and widespread enhancer reprogramming by the oncogenic fusion protein EWS-FLI1. Cell Rep. 10,1082–1095. [PubMed: 25704812]

Versteege I, Sévenet N, Lange J, Rousseau-Merck MF, Ambros P, Handgretinger R, Aurias A, and Delattre O. (1998). Truncating mutations of hSNF5/INI1 in aggressive paediatric cancer. Nature 394, 203–206. [PubMed: 9671307]

Zhang Y, Liu T, Meyer CA, Eeckhoute J, Johnson DS, Bernstein BE, Nusbaum C, Myers RM, Brown M, Li W, and Liu XS (2008). Model- based analysis of ChIP-seq (MACS). Genome Biol. 9, R137.

Highlights

- EWS-FLI1 binds and recruits BAF complexes to GGAA microsatellites in Ewing sarcoma
- De novo enhancer activation at GGAA repeats is a neomorphic property of EWS-FLI1
- The EWS-FLI1 PrLD is necessary for phase transitions and de novo enhancer activation
- Small PrLD fragments fused to FLI1 are sufficient to recapitulate EWS-FLI1 activity

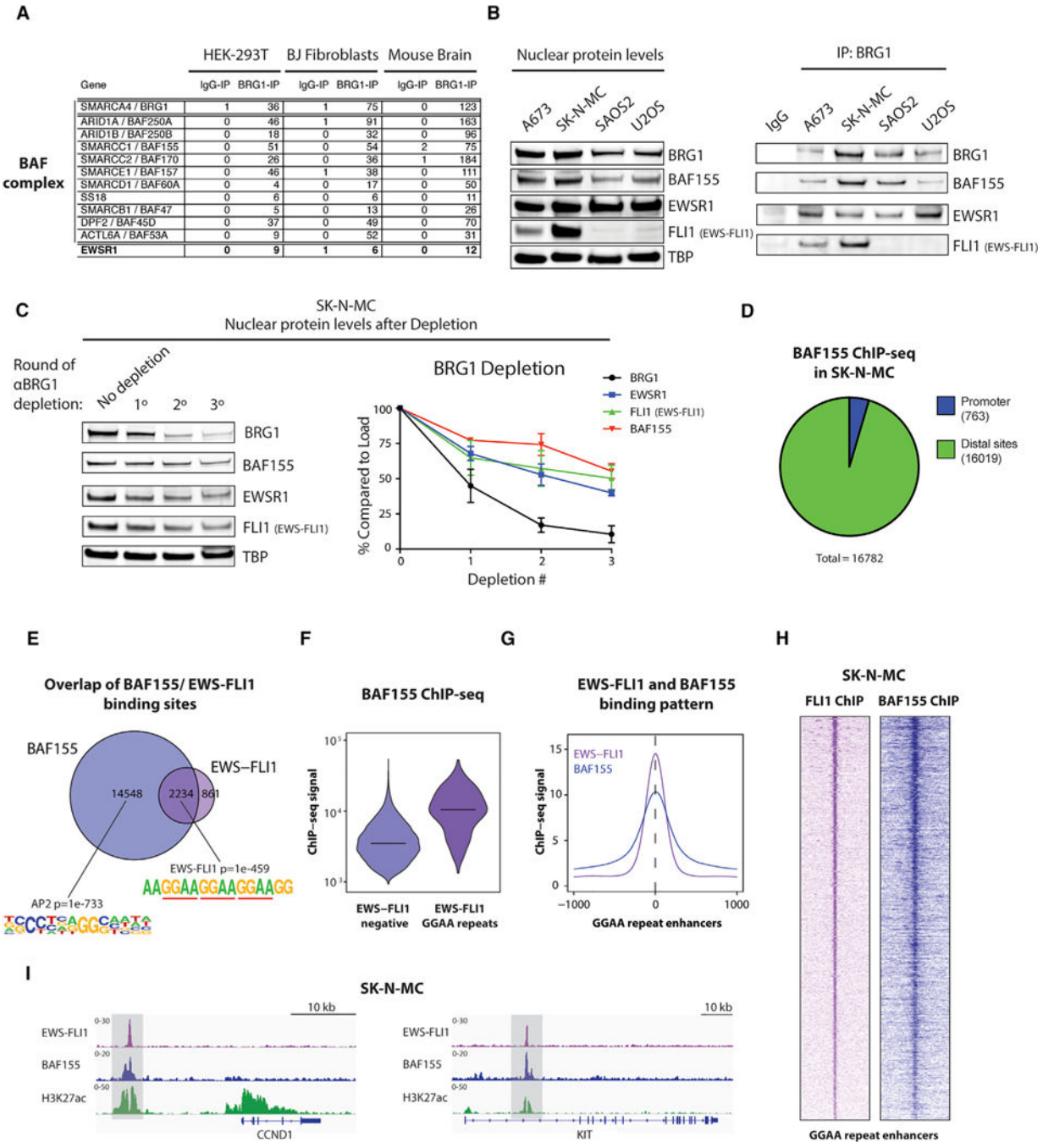

Figure 1. EWS-FLI1 Binds mSWI/SNF (BAF) Complexes and Co-localizes at Tumor-Specific GGAA Repeat Enhancer Elements in Ewing Sarcoma

(A) Table highlighting enrichment of EWSR1 peptides in anti-BRG1 immunoprecipitation/ mass spectrometry studies in human cells (HEK293-T and BJ fibroblasts) and in mouse brain tissue. Highlighted is the number of peptides of EWSR1 and BAF complex members. (B) (Left) Immunoblotting for BAF subunits, EWSR1 and EWS-FLI1, performed on nuclear extracts used for immunoprecipitation. (Right) Immunoprecipitation studies using an anti-BRG1 antibody in Ewing sarcoma (A673 and SK-N-MC) and osteosarcoma (SAOS2 and

U2OS) cell lines demonstrate binding of EWSR1 (wild-type) and EWS-FLI1 to BAF complexes.

(C) (Left) Immunodepletion studies performed on SK-N-MC Ewing sarcoma nuclear extracts using an anti-BRG1 antibody. (Right) Quantification of depletion experiments using quantitative densitometry is shown. Error bars represent SEM of n = 2 independent experiments.

(D) Distribution of MACS-called BAF155 ChIP-seq peaks in SK-N-MC Ewing sarcoma cells. BAF complexes (as marked by BAF155) are primarily localized at putative enhancer sites. Promoters are annotated using the Refseq promoter database.

(E) Venn diagram depicting the overlap of BAF155 and EWS-FLI1 (FLI1) MACS-called peaks in Ewing sarcoma SK-N-MC cells. The top motifs for distal sites with BAF155-only or BAF155/EWS-FLI1 overlap are shown.

(F) Total BAF155 ChIP-seq signals at BAF-155-only sites (n = 14,548) and sites co-bound with EWS-FLI1 at GGAA repeats (n = 660) as represented by violin plots.

(G) Composite plot shows EWS-FLI1 and BAF155 ChIP-seq signals at overlapping GGAA repeat binding sites. The x axis represents a 2-kb window centered on EWS-FLI1 binding sites.

(H) Heatmaps showing EWS-FLI1 and BAF155 ChIP-seq signal density in Ewing sarcoma SK-N-MC cells. 10-kb windows in each panel are centered on EWSFLI1-bound GGAA repeat enhancer sites (n = 812).

(I) Representative examples of EWS-FLI1 and BAF155 co-occupancy shown at GGAA repeat enhancers associated with the *CCND1* and *KIT* genes. Enhancer regions are highlighted in light gray.

See also Figure S1.

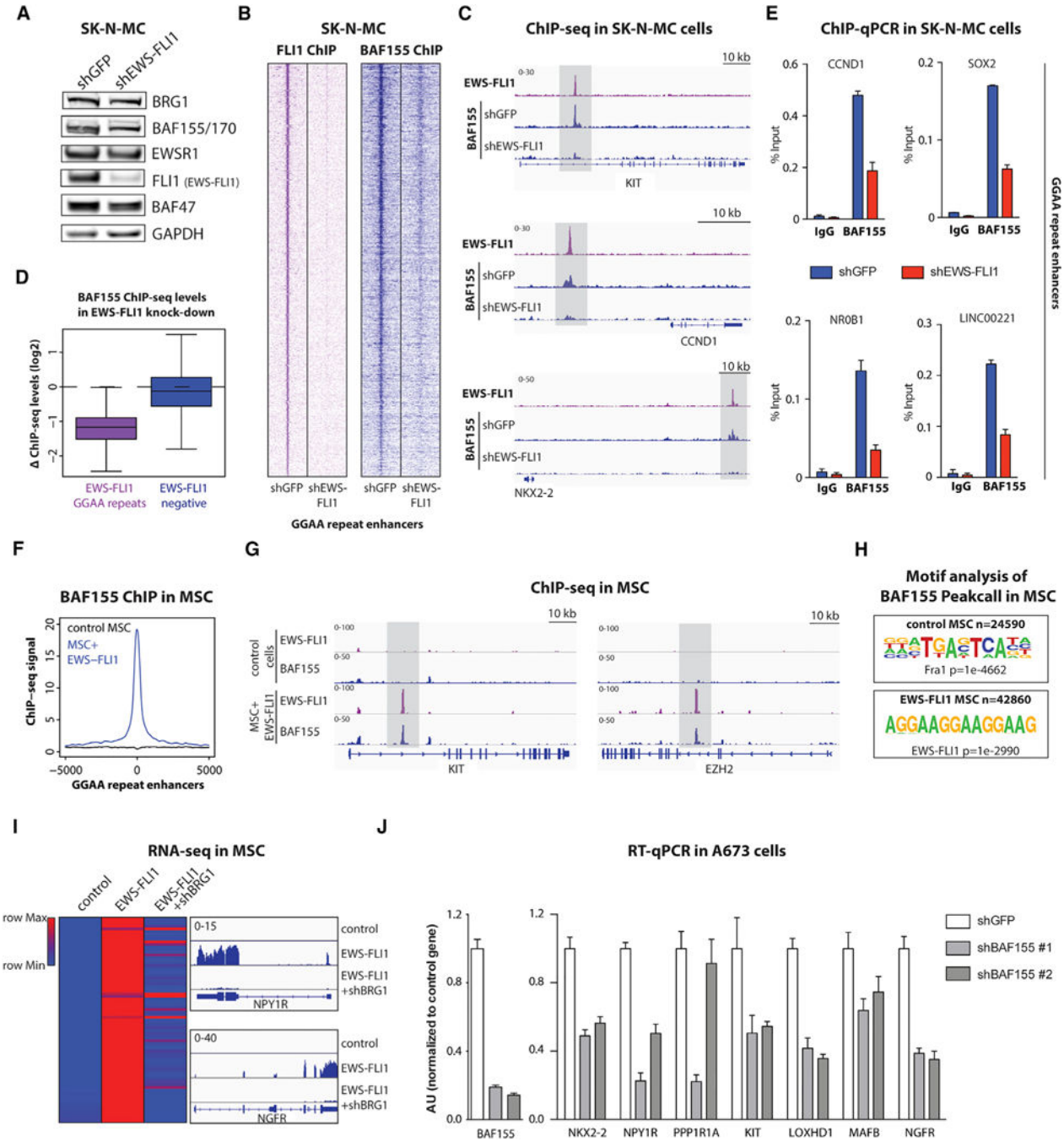

Figure 2. Interdependency of EWS-FLI1 and BAF Complexes in Driving Oncogenic Gene Expression Programs in Ewing Sarcoma

(A) shRNA-mediated suppression of EWS-FLI1 (versus shGFP as control) in SK-N-MC Ewing sarcoma cells; immunoblot for FLI1 (EWS-FLI1), EWSR1, and BAF complex subunits performed on nuclear extracts.

(B) Heatmaps showing EWS-FLI1 and BAF155 ChIP-seq signal density in SK-N-MC cells treated with either shGFP control or shEWS-FLI1 knockdown. 10-kb windows in each panel are centered on EWS-FLI1-bound GGAA repeat enhancer sites (n = 812).

(C) Example tracks demonstrating decreased binding of BAF155 at EWS-FLI1-bound GGAA repeat enhancers associated with *KIT, CCND1,* and *NKX2–2* in SK- N-MC cells treated with either shGFP or shEWS-FLI1 knockdown. Enhancer regions of interest are highlighted in light gray.

(D) BAF155 occupancy is decreased specifically at GGAA repeat regions following EWS-FLI1 knockdown in SK-N-MC cells. Boxplots depict the changes in BAF155 ChIP-seq signals between SK-N-MC cells treated with either shGFP or shEWS-FLI1 knockdown. BAF155 MACS-called peaks are divided into EWS-FLI1-bound GGAA repeat enhancers (n = 660 sites, purple) and BAF155-only sites (n = 14,548 peaks, blue).

(E) ChIP-qPCR validation of decreased BAF155 occupancy at selected EWS-FLI1 GGAA repeat enhancers associated with *CCND1, SOX2, NR0B1*, and *LINC00221*. Error bars indicate SD of three technical replicates and represent at least two independent biological experiments.

(F) Introduction of EWS-FLI1 in MSCs results in recruitment of BAF complexes to GGAA microsatellite repeats. Composite plot shows BAF155 ChIP-seq signals in control MSCs (black) and EWS-FLI1-expressing MSCs (blue). The x axis represents a 10-kb window centered on EWS-FLI1 binding sites.

(G) Examples of recruitment of BAF155 by EWS-FLI1. ChIP-seq tracks illustrate EWS-FLI1 and BAF155 binding at GGAA repeat microsatellites upon introduction of EWS-FLI1 into MSCs. Enhancer regions of interest are highlighted in light gray.

(H) Motif analysis on BAF155 MACS-called peaks in control conditions and on newly created peaks after EWS-FLI1 expression in MSCs.

(I) BAF complex activity is required for activation of EWS-FLI1 target genes. (Left) Heatmap shows relative RNA-seq gene expression levels of genes associated with GGAA repeats and activated upon introduction of EWS-FLI1 in MSCs (rows, n = 79 genes). The columns show MSCs treated with either empty vector control, EWS-FLI1 + shGFP, or EWS-FLI1+ shBRG1. Expression values were normalized by row. (Right) Example RNA-seq tracks over selected genes are shown.

(J) RT-qPCR experiments show decreased mRNA expression of EWS-FLI1 target genes 48 hr post-infection with BAF155 shRNA in A673 Ewing sarcoma cells. Error bars indicate SD of three technical replicates and represent at least two independent biological experiments. See also Figure S2.

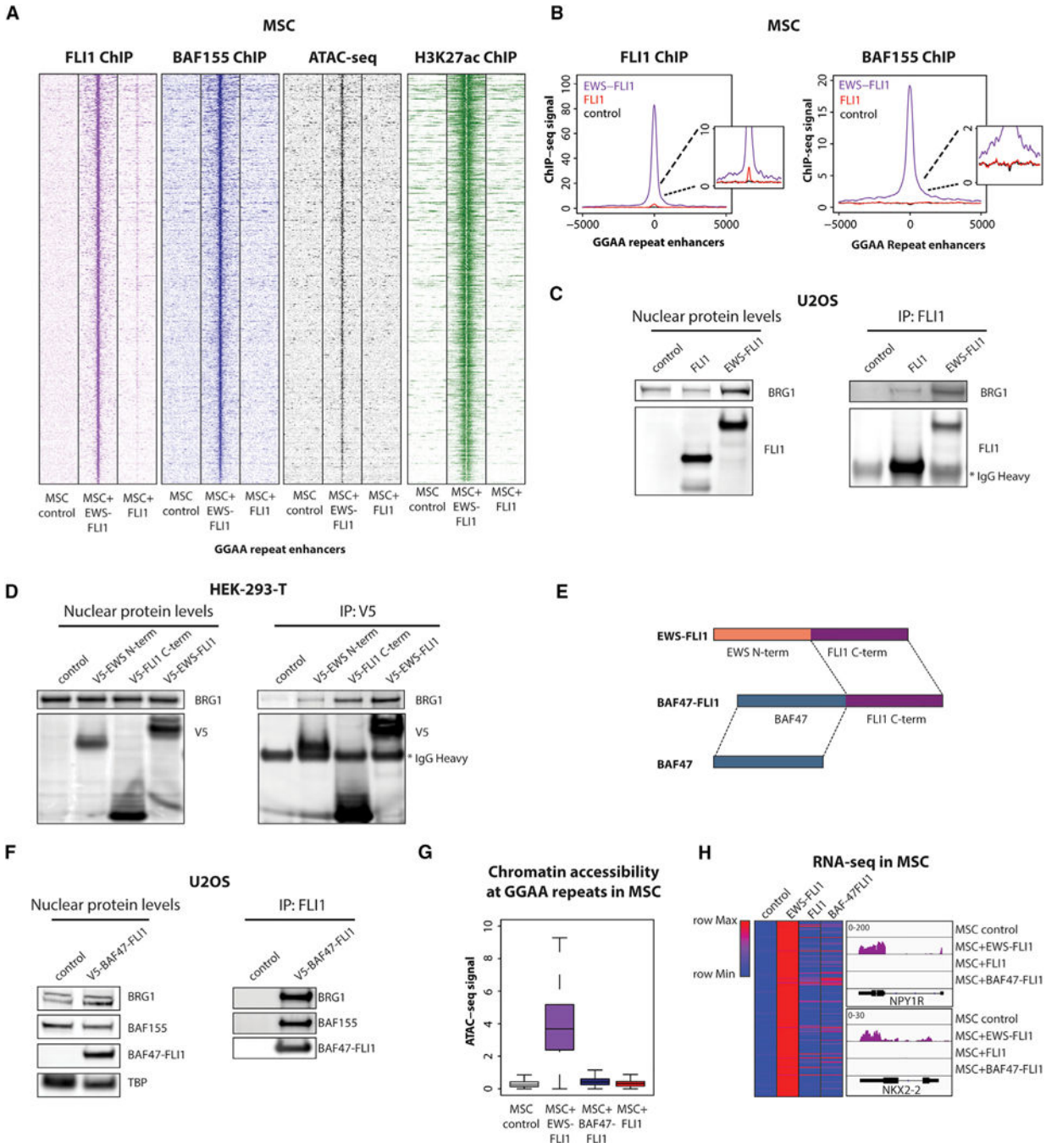

Figure 3. Recruitment of BAF Complexes to GGAA Microsatellite Repeats Is a Neomorphic Property of EWS-FLI1

(A) Heatmaps of FLI1, BAF155, H3K27ac ChIP-seq, and ATAC-seq signal densities in MSCs infected with either control vector, EWS-FLI1, or wild-type FLI1. 10-kb windows in each panel are centered on EWS-FLI1-bound GGAA repeat enhancer sites (n = 812).

(B) Composite plots show FLI1 (left) and BAF155 (right) ChIP-seq occupancy over GGAA repeat enhancers in control MSCs and MSCs expressing EWS-FLI1 or FLI1. The x axis represents a 10-kb window centered on EWS-FLI1 binding sites. Inset: 10-fold

magnification shows minimal wild-type FLI1 binding over repeat enhancers but no BAF155 recruitment by FLI1.

(C) Bothwild-typeFLI1 and EWS-FLI1 interactwith BAFcomplexes.(Left) Immunoblotsfrom nuclearextractsshowlentiviral expression ofwild-typeFLI1 orEWS-FLI1 and the levels of endogenous BRG1 in U2OS cells. (Right) Co-immunoprecipitation experiments using anti-FLI1 antibodies show interactions with BAF. * indicates immunoglobulin G (IgG) heavy chains used for immunoprecipitation.

(D) EWS-FLI1 interacts with BAF complexes through both EWS N-terminal and FLI1 C-terminal fragments. (Left) Immunoblots from nuclear extracts show the expression of transiently transfected V5-EWSR1 N-terminal, V5-FLI1 C-terminal, or V5-EWS-FLI1 and the levels of endogenous BRG1 in HEK293-T cells. (Right) Co-immunoprecipitation experiments using anti-V5 antibodies show interactions with BAF. * indicates IgG heavy chains used for immunoprecipitation.

(E) Schematic of the BAF47-FLI1 fusion protein used in experiments in relation to EWS-FLI1 and BAF47.

(F) (Left) Immunoblots from nuclear extracts show lentiviral expression of BAF47-FLI1 fusion protein and the levels of endogenous BAF proteins in U2OS cells. (Right) Anti-FLI1 immunoprecipitation confirms an interaction between BAF47-FLI1 and BAF complex subunits.

(G) ATAC-seq signal intensity indicative of chromatin accessibility at GGAA repeat microsatellites in MSCs infected with either control vector, EWS-FLI1, BAF47- FLI1, or FLI1 wild-type.

(H) The fusion of the FLI1 C-terminal region to BAF47 is not sufficient for the activation of EWS-FLI1 target genes. Heatmap shows relative RNA-seq gene expression levels of genes associated with GGAA repeats and activated upon introduction of EWS-FLI1 in MSCs (rows, n = 207 genes). The columns show MSCs treated with either control vector, EWS-FLI1, wild-type FLI1, or BAF47-FLI1. Expression values were normalized by row. (Right) Example RNA-seq tracks over selected genes are shown.

See also Figures S3 and S4.

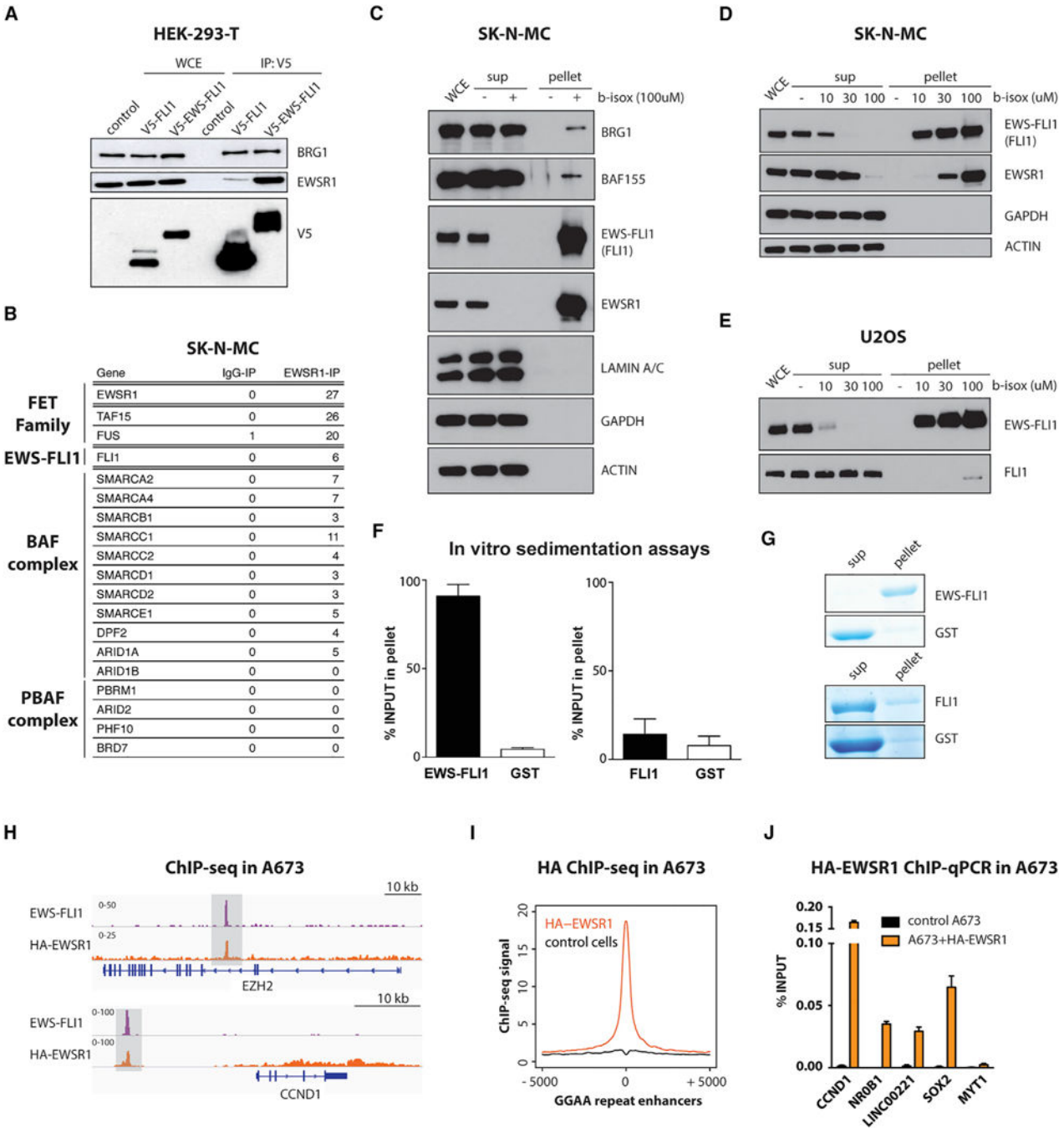

Figure 4. Fusion of EWSR1 to FLI1 Confers Multimerization and Phase Transition Properties

(A) Endogenous wild-type EWSR1 strongly interacts with EWS-FLI1 compared to wild-type FLI1. Immunoblots of whole-cell extract and anti-V5 immunopre- cipitates from 293T cells transfected with either control vector, V5-FLI1, or V5-EWS-FLI1 are shown.

(B) Proteomic mass spectrometry of IgG and anti-EWSR1 immunoprecipitations performed in SK-N-MC cells. Table shows the number of unique peptides in each condition.

(C-E) EWS-FLI1 has a strong ability to precipitate in presence of b-isox compared to wild-type FLI1. (C) EWS-FLI1 precipitates in presence of 100 μM b-isox in Ewing sarcoma cell

lysates. (D) EWS-FLI1 precipitates upon treatment with b-isox in a dose-dependent manner in Ewing sarcoma cell lysates. (E) Lentivirally expressed EWS-FLI1, but not wild-type FLI1, precipitates upon treatment with b-isox in U2OS osteosarcoma cell lysates.
(F and G) In vitro sedimentation assays from bacterially expressed and purified EWS-FLI1 or wild-type FLI1. (F) Quantification oftwo independent experiments is shown.(G) Representativeexamplesofinvitrosedimentationassaysareshown.TheGSTtagiscleaved as partoftheassayandisused asasolubleinternalcontrol.
(H-J) EWSR1 is recruited to EWS-FLI1-bound GGAA repeat enhancers in Ewing Sarcoma. (H) Example ChIP-seq tracks show co-occupancy of EWS-FLI1 and HA-EWSR1 at GGAA repeat enhancers in A673 cells. Regions of co-occupancy are highlighted in light gray. (I) Composite plot shows HA-EWSR1 binding at EWSFLI1 GGAA repeat enhancers in A673 cells. A 10-kb window centered on EWS-FLI1-bound repeat enhancer is shown. (J) ChIP-qPCR experiments validate HA-EWSR1 binding at EWS-FLI1 GGAA repeat enhancers associated with *CCND1, SOX2, NR0B1*, and *LINC00221*, but not a control region near *MYT1*.
See also Figure S5.

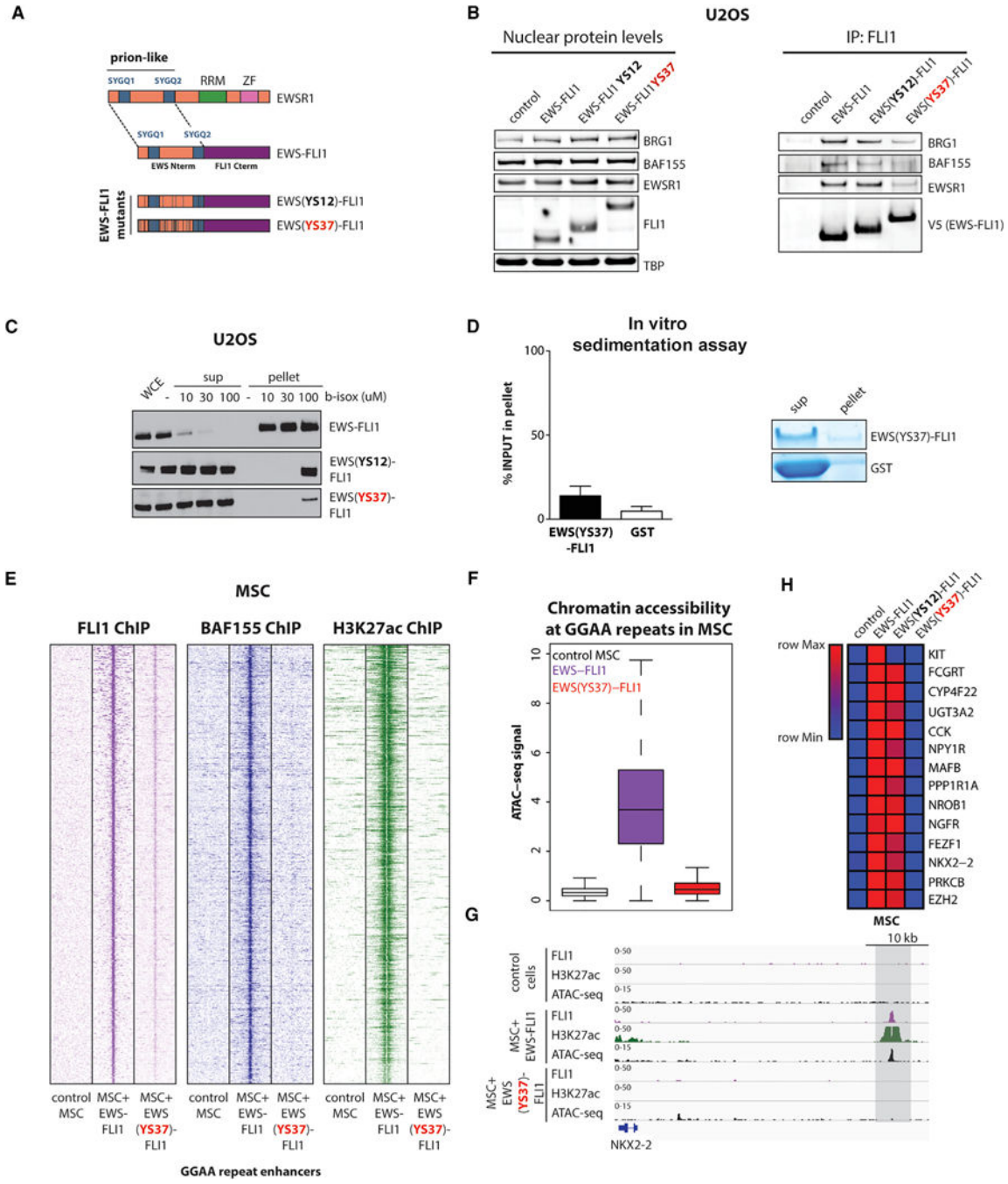

Figure 5. Tyrosine Residues in the EWS-FLI1 Prion-like Domain Are Necessary for DNA Binding at GGAA Microsatellites and Enhancer Induction

(A) Schematics of EWSR1, EWS-FLI1, and EWS-FLI1 tyrosine mutant variants used in experiments. Tyrosines (Y) mutated into serines (S) are shown as black bars within the EWS N-terminal prion-like domain. Mutants contained either 12 (YS12) or 37 (YS37) Y to S mutations. See also Figure S6A.

(B) (Left) Immunoblots show nuclear input levels of EWSR1 and BAF proteins and the lentiviral expression of EWS-FLI1, EWS(YS12)-FLI1, or EWS(YS37)-FLI1 mutants in U2OS cells. (Right) Co-immunoprecipitation experiments using anti-FLI1 antibodies reveal

that the EWS(YS37)-FLI1 mutant exhibits decreased interactions with wild-type EWSR1 and BRG1.

(C) Dose-dependent b-isox precipitation assay after lentiviral expression of either EWS-FLI1 or mutants EWS(YS12)-FLI1 or EWS(YS37)-FLI1 in U2OS cells.

(D) In vitro sedimentation assay from bacterially expressed and purified EWS(YS37)-FLI1. (Left) Quantification of two independent experiments is shown. (Right) Representative examples of in vitro sedimentation assays are shown. The GST tag is cleaved as part of the assay and is used as a soluble internal control.

(E) Heatmaps of FLI1, BAF155, and H3K27ac ChIP-seq signal densities in MSCs treated with either control vector, EWS-FLI1, or EWS(Y37)-FLI1 mutant. 10-kb windows in each panel are centered on EWS-FLI1-bound GGAA repeat enhancer sites (n = 812).

(F) ATAC-seq signal intensity indicative of chromatin accessibility at GGAA repeat microsatellites in MSCs infected with either control, EWS-FLI1, or EWS(YS37)-FLI1 mutant.

(G) Representative example ChIP-seq tracks of FLI1 (EWS-FLI1), H3K27Ac, and ATAC-seq signals over the NKX2–2 locus in MSCs expressing either control, EWS-FLI1, or EWS(YS37)-FLI1 mutant.

(H) Heatmap shows changes in expression detected by RT-qPCR for selected EWS-FLI1 target genes associated with GGAA repeats after infection of MSCs with either control vector, EWS-FLI1, EWS(YS12)-FLI1, or EWS(YS37)-FLI1 mutants.

See also Figure S6.

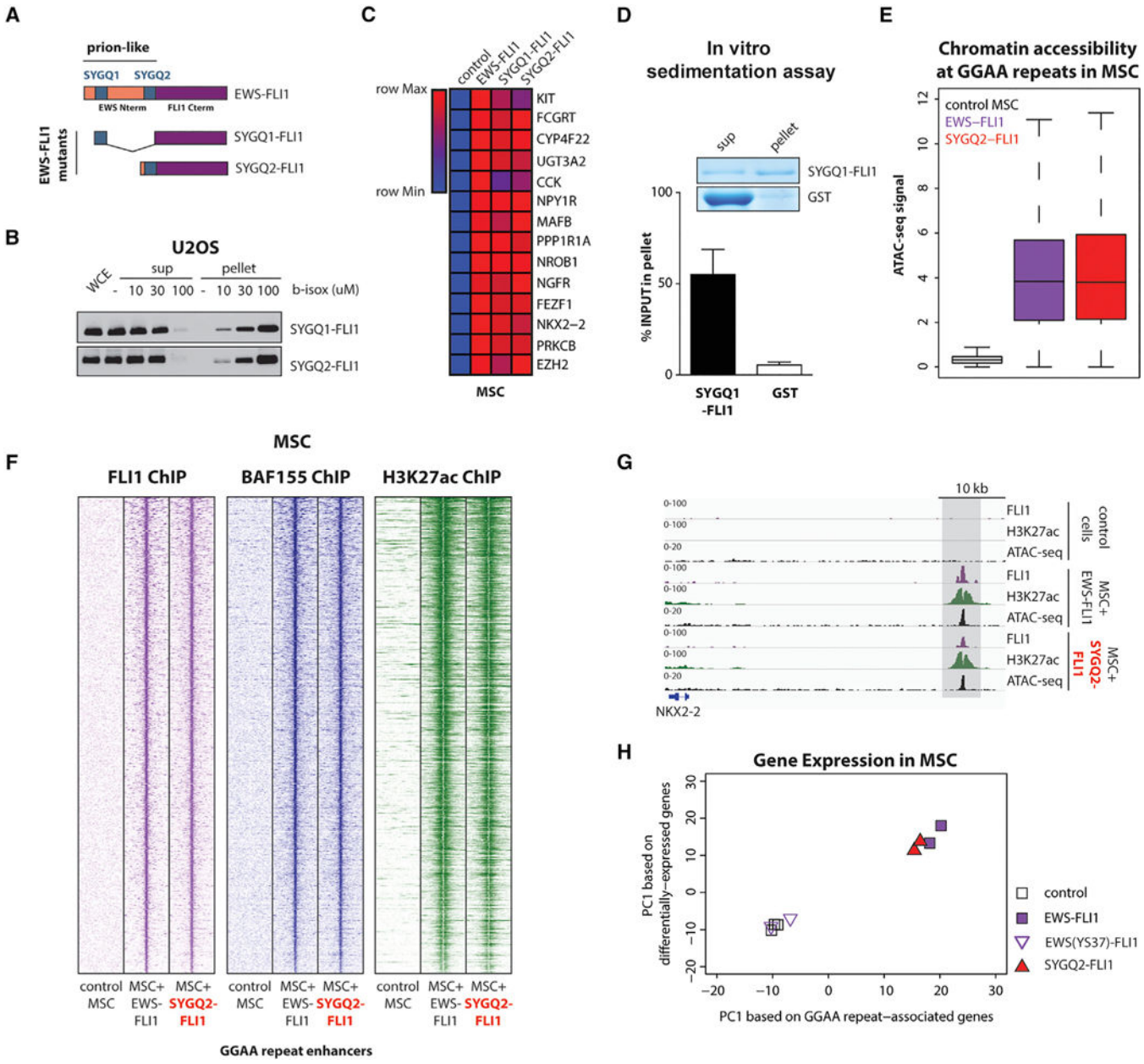

Figure 6. Fusion of Fragments of the EWSR1 Prion-like Domain to the FLI1 C Terminus Is Sufficient to Recapitulate EWS-FLI1 Activity

(A) Schematic representation of EWS-FLI1 prion-like domain mutants used in experiments. SYGQ1 or SYGQ2 fragments are fused to the FLI1 C terminus.

(B) Dose-dependent precipitation assay in presence of b-isox after lentiviral expression of fusion proteins in U2OS cells.

(C)Heatmap shows changes in expression detected by RT-Qpcr for selected EWS-FLI1 target genes associated with GGAA repeats after infection of MSCs with either control vector, EWS-FLI1, SYGQ1-FLI1, or SYGQ2-FLI1 fusion proteins.

(D) In vitro sedimentation assay from bacterially expressed and purified SYGQ1-FLI1. (Top) Representative examples of invitro sedimentation assays are shown. The GST tag is

cleaved as part of the assay and is used as a soluble internal control. (Bottom) Quantification of two independent experiments is shown.

(E) ATAC-seq signal intensity indicative of chromatin accessibility at GGAA repeat microsatellites in MSCs infected with either control, EWS-FLI1, or the SYGQ2-FLI1 fusion protein.

(F) Heatmaps of FLI1, BAF155, and H3K27ac ChIP-seq signal densities in MSCs treated with either control vector, EWS-FLI1, or the SYGQ2-FLI1 fusion protein. 10-kb windows in each panel are centered on EWS-FLI1-bound GGAA repeat enhancer sites (n = 812).

(G) Example ChIP-seq tracks of FLI1 (EWS-FLI1), H3K27Ac, and ATAC-seq signals over the NKX2–2 locus in MSCs expressing either control, EWS-FLI1, or the SYGQ2-FLI1 fusion protein.

(H) Principal-component analysis (PCA) plot showing PC1 for the 207 target genes associated with EWS-FLI1 GGAA repeats sites (x axis) and PC1 for the 158 remaining differentially expressed genes in EWS-FLI1-expressing cells (y axis). RNA-seq datasets are from MSCs infected with either control vector, EWS-FLI1, EWS(YS37)-FLI1, or the SYGQ2-FLI1 fusion protein.

See also Figure S7.

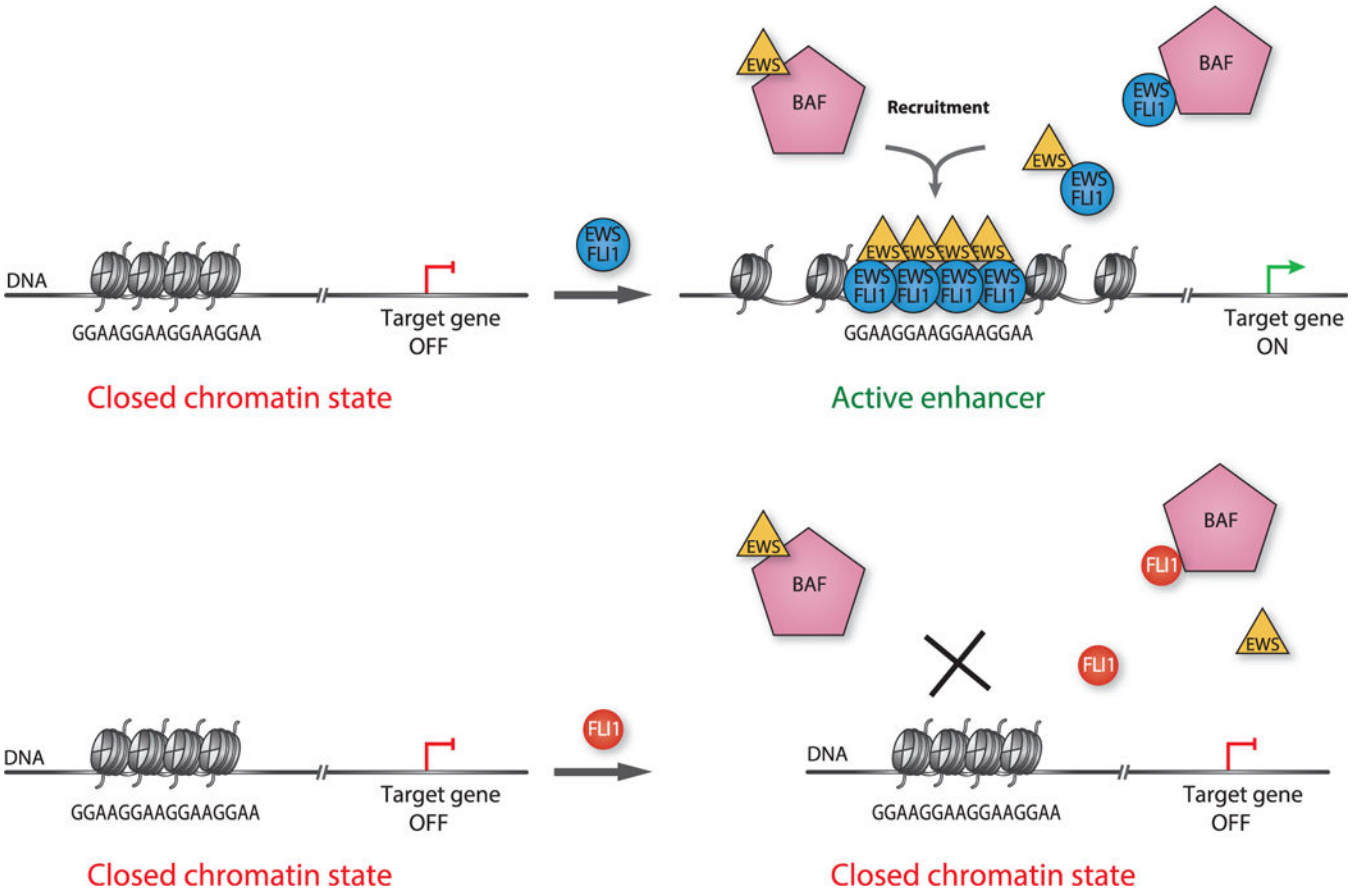

Figure 7. Model for EWS-FLI1 Binding at GGAA Repeat Microsatellites and Enhancer Activation in Ewing Sarcoma

(Top) In presence of EWS-FLI1, multimerization is required for stable binding at GGAA repeats and recruitment of BAFcomplexes. (Bottom)Wild-type FLI1 cannot stably bind at GGAA repeats.

KEY RESOURCES TABLE

REAGENT or RESOURCE	SOURCE	IDENTIFIER
Antibodies		
Antibodies used for immunoblotting and immunoprecipitation	N/A	See Table S1
Antibodies used for ChIP	N/A	See Table S1
Chemicals, Peptides, and Recombinant Proteins		
HALT PROTEASE AND PHOSPHATASE inhibitors	Pierce	Cat#PI78445
Dynabeads® Protein G	LIFE TECHNOLOGIES	Cat#10004D
Biotinylated isoxazole (b-isox)	SIGMA ALDRICH	Cat#T511617–1MG
PDGF-BB	PeproTech	Cat#50589827
TransIT-LT1 Transfection Reagent	MIRUS BIO LLC	Cat#MIR 2305
Polybrene (HEXADIMETHRINE BROMIDE)	Sigma-Aldrich	Cat#H9268–50G
Puromycin	FISHER SCIENTIFIC	Cat#NC9138068
Blasticidin	FISHER SCIENTIFIC	Cat#NC9016621
Western Lightning Western Blot Chemiluminescence Reagent Plus	PERKINELMER	Cat#NEL104001EA
AUTORAD BLUE FILM	FISHER SCIENTIFIC	Cat#NC9648989
RNase A	ROCHE	Cat#11119915001
Proteinase K	LIFE TECHNOLOGIES	Cat#25530049
Palbociclib (PD 0332991 ISETHIONATE)	SIGMA ALDRICH	Cat#PZ0199
PRESCISSION PROTEASE	FISHER SCIENTIFIC	Cat#45001319
GLUTATHIONE SEPHAROSE 4B	FISHER SCIENTIFIC	Cat#45000139
D(+)TREHALOSE	SIGMA ALDRICH	Cat#T9531
Critical Commercial Assays		
TruSeq Stranded Total RNA Library Prep Kit with Ribo-Zero Gold Set A	Illumina	Cat#RS-122–2301
TruSeq Stranded Total RNA Library Prep Kit with Ribo-Zero Gold Set B	Illumina	Cat#RS-122–2302
Nextera DNA Sample Preparation Kit	Illumina	Cat#FC-121–1030
Nucleospin RNA Plus	Clontech	Cat#740984.50
Celltiter-Glo Luminescent cell viability assay	Promega	Cat#G7570
fast SYBR Green Master Mix	ThermoFisher	Cat#4385618
High Capacity cDNA reverse transcription kit	ThermoFisher	Cat#4387406
Deposited Data		
ChIP-seq, RNA-seq, ATAC-seq data	This study	GEO: GSE94278
Raw and analyzed data	Riggi et al., 2014	GEO: GSE61953
Experimental Models: Cell Lines		
A673	ATCC	CRL-1598
SK-N-MC	ATCC	HTB-10

REAGENT or RESOURCE	SOURCE	IDENTIFIER
U20S	ATCC	HTB-96
HEK293-T	ATCC	CRL-11268
HEK293-T LentiX	Clontech	Cat#632180
Human pediatric Mesenchymal Stem Cells	This study	N/A
Experimental Models: Organisms/Strains		
BL21(DE3)LYSS	FISHER SCIENTIFIC	Cat#PRL1195
Oligonucleotides		
Primers for RT-qPCR	IDT	See Table S1
Primers for ChIP-qPCR	IDT	See Table S1
Recombinant DNA		
pLIV-V5-EWS-FLI1	This study	N/A
pLIV-V5-FLI1	This study	N/A
N106-BAF47-FLI1	This study	N/A
pLIV-HA-EWSR1	This study	N/A
N106-GFP-EWSR1	This study	N/A
pLIV-V5-EWS(YS12)-FL11	This study	N/A
pLIV-V5-EWS(YS37)-FL11	This study	N/A
pLIV-V5-SYGQ1-FLI1	This study	N/A
pLIV-V5-SYGQ2-FLI1	This study	N/A
pLIV-V5-EWS(ASYGQ1)-FLI1	This study	N/A
pLIV-V5-EWS(ASYGQ2)-FLI1	This study	N/A
pLIV-V5-EWS(DSYGQ1 DSYGQ2)-FLI1	This study	N/A
pLIV-V5-EWS N-terminal	This study	N/A
pLIV-V5-FLI1 C-terminal	This study	N/A
pINDUCER-GFP	This study	N/A
pINDUCER- V5-EWS-FLI1	This study	N/A
pINDUCER- EWS(YS37)-FLI1	This study	N/A
pINDUCER- SYGQ2-FLI1	This study	N/A
pGEX-6P1-V5-EWS-FLI1	This study	N/A
pGEX-6P1-V5-FLI1	This study	N/A
pGEX-6P1 - V5-EWS(YS37)-FLI1	This study	N/A
pGEX-6P1 - V5-SYGQ1-FLI1	This study	N/A
shRNA targeting sequence: BRG1 GGCATAGGCCTTAGCAGTAAC	Broad Institute	Clone ID: TRCN0000231102
shRNA targeting sequence: BRG1 CTTTGCGTATCGCGGCTTTAA	Broad Institute	Clone ID: TRCN0000231101
shRNA targeting sequence: BAF155#1 CCCACCACATTTACCCATATT	Broad Institute	Clone ID: TRCN0000015629
shRNA targeting sequence: BAF155#2 GCAGGATATTAGCTCCTTATA	Broad Institute	Clone ID: TRCN0000015628
shRNA targeting sequence: EWS-FLI1 CGTCATGTTCTGGTTTGAGAT	Broad Institute	Clone ID: TRCN0000005322

REAGENT or RESOURCE	SOURCE	IDENTIFIER
Software and Algorithms		
bwa	Li and Durbin, 2009	https://github.com/lh3/bwa
bwtool	Pohl and Beato, 2014	https://github.com/CRG-Barcelona/bwtool
STAR	Dobin et al., 2013	https://github.com/alexdobin/STAR
MACS2	Zhang et al., 2008	https://github.com/taoliu/MACS
Prism 6	Graphpad	N/A
R	version 3.2.3	https://cran.r-project.org
IGV	IGV_2.3.60	https://github.com/igvteam/igv
HOMER	Heinz et al., 2010	http://homer.salk.edu/homer/
DESeq2	Love et al., 2014	https://bioc.ism.ac.jp/packages/3.1/bioc/html/DESeq2.html
bedtools	Quinlan and Hall, 2010	https://github.com/arq5x/bedtools
featureCounts	Liao et al., 2014	http://subread.sourceforge.net
ImageJ v1.50i Other	National Institutes of Health, USA	http://imagej.nih.gov/ij
Other		